Mechanical Loss of Crystal Fibres for Torsion Pendulum Experiments
(ねじれ振り子における 単結晶ファイバの機械損失)

by

Ooi Ching Pin

A thesis submitted in partial fulfilment for the
Master of Science

The University of Tokyo
Graduate School of Science
Department of Physics

August 2018

Abstract

Thermal noise generated from mechanical loss in torsion pendulums creates a hard limit in the sensitivity of any measurement utilising them. Characterising and mitigation of this noise source would allow for more accurate measurements in a variety of experiments. Here, the torsional Q of 1 mm thick sapphire fibres were measured, with the maximum value of $Q = 1.3 \times 10^5$ at 1.31 Hz measured for an unpolished fibre. This is in line with the expected value extrapolated from previous studies for Q limited by surface losses, and is the highest ever measured value for a sapphire fibre at room temperature, as far as the author knows.

Acknowledgements

I would like to thank my supervisor, Associate Professor Ando Masaki, Assistant Professor Michimura Yuta and the fellow students in the research laboratory for taking their time and energy in guiding and helping me with this project, as well putting up with my terrible Japanese. Thanks must also be given to Shimozawa Togo at the machining lab for helping build the parts needed for this study, as well as Gobind Singh for helping me out with my many requests relating to this project.

I would also like to thank my family and friends for their encouragement and support, especially those who took the time and money to visit me in Tokyo. I would also like to acknowledge the the Graduate School of Science of the University of Tokyo for their support via the global science graduate course, without which this work would not have been plausible. Last but not least, I would like to acknowledge the importance of Tokyo's world-class food scene, which has carried me though many dark days and gave me the strength to carry on.

Contents

List of Symbols

G	universal gravitational constant
Q	Q factor
x	position
$\dot{x}$	velocity
$\ddot{x}$	acceleration
t	time
F	force
k_B	Boltzmann's constant
τ_s	shear stress
μ	shear modulus
γ	strain angle
r	radius (various)
R	radius of fibre
D	diameter of fibre
θ	angle of twist of fibre
l	length (various)
L	length of fibre
M	moment (torque)
A	area
J	second moment of area
i	$\sqrt{-1}$
τ	time constant
Y	Young's modulus
ν	Poisson's ratio
κ	angular spring constant

I	moment of inertia
ω	angular frequency
ω_0	angular resonance frequency
f	frequency
f_0	resonance frequency
$\Re()$	the real part of ()
Z	generalised impedance
$\hbar$	reduced Plank's constant
Y	generalised admittance
$\hbar$	reduced Plank's constant
T	temperature
E	energy
m	mass
b	velocity linked damping coefficient
k	spring constant
ϕ	loss angle
S	surface
V	volume
a	amplitude
g	Earth's gravitational field strength
$W()$	the Lambert W function
π	pi
Δ_r	relaxation strength
τ_r	relaxation time
α	coefficient of thermal expansion
c	volumetric heat capacity
λ	thermal conductivity
ℓ	angular momentum
n	number density
C	dimensionless shape constant
ρ	density
β	phase angle
d	pendulum length difference

Chapter 1

Introduction

This work, as the title suggests, is about mechanical loss in torsion pendulums, specifically that of from the suspension. This mechanical loss leads to thermal noise, which limits the sensitivity of precision experiments.

1.1 Torsion Pendulums

The torsion pendulum, also known as the torsion balance, is a pendulum that oscillates by twisting about its wire, as compared to the standard pendulum which swings in response to gravity. The general underlying motivation behind using such a device is simple; the desire to eliminate (or at least reduce significantly) the effects of Earth's gravity on whatever force being measured.

This device has a long and storied history in classical physics, with most famous examples being the usage by Charles-Augustin de Coulomb and Henry Cavendish [1] to establish Coulomb's law and the universal gravitational constant (G) respectively. These are the first two recorded usage of the torsional pendulum for metrology, with Cavendish attributing the invention to Rev. John Michell (of the Royal Society of London), even with Coulomb's experiments being published first. This suggest that it was independently invented by Coulomb. In recent years, notable uses of the torsion pendulum include the ground-based testing of Laser Interferometer Space Antenna (LISA) gravitational sensors [2], as well as for ever more accurate measurements of G, which has eluded the accuracy of most other physical constants [3].

1.1.1 Torsion-Bar Antenna (TOBA)

The main motivation behind this work, the Torsion-Bar Antenna (TOBA) is a proposed ground based gravitational wave detector [4]. It is a torsion pendulum with nominally has 10 m long bars, which rotate via tidal forces caused by gravity waves. In order for the design to successful, noise must be sufficiently lowered to be able to detect the faint signals of gravitational waves. One of the main noise sources is that of thermal noise, which this work focuses on. The aim is to lower the suspension thermal noise to below the quantum noise, and thus remove it from being a limiting noise source in the sensitivity. This work is essentially a proof of concept in achieving the properties required for TOBA to reach its target sensitivity.

1.2 Thermal Noise

Thermal noise manifests from dissipative systems (including mechanical loss), and is a consequence of the second law of thermodynamics. This creates a limit in sensitivity in mechanical systems, and for torsion pendulums, is caused by loss mainly though the suspension wire due to energy being dissipated as it turns from potential to kinetic energy. Of cause, the torsion mass itself will also have thermal noise associated with it, but in general will be much smaller and less less of an issue. In order to reduce it, choosing the appropriate material is essential. To quantify mechanical loss and thus thermal noise, we use a dimensionless figure of merit Q, in which the higher it is, the lower the loss (outside of resonance).

In this quest to lower mechanical noise, the quest to measure the intrinsic Q of materials were started. Most metals have an intrinsic Q of 10^4 before annealing and 10^5 after annealing [5, 6], while crystalline materials, such as quartz, sapphire, silicon were found to have higher Q of around 10^8 [7, 8]. For the use as fibres in suspension systems, much research were carried out, mainly for pendulum systems. Much of the progress in the field was carried out in the effort to reach the target noise sensitivity for the suspension system. In particular, fused silica, which is currently used as for suspending the test masses at aLIGO [9] and Advanced Virgo, received much attention. Most of these studies involved the flexural modes of cantilevers. Unfortunately, there have only been a few studies done for torsion pendulums, leading to a gap in knowledge. This problem is especially acute in the case of TOBA, where the required Q to hit the target sensitivity has not been demonstrated in any previous experiment. This unfortunate state of affairs stem form two

main reasons; firstly, there is no simple way to excite the torsion mode of a simple beam, and secondly, there has not been a big push on R&D in this specific area.

1.3 Experiment

While there have been many studies on the intrinsic values of internal friction of various materials [7, 10, 11], there is a lack of data on actual measurements on *torsion* modes, especially with respect to fibres. In particular, there is a lack of measurements at low frequencies and in the presence of loads.

The experiments done here are therefore to experimentally verify if crystalline suspension fibres would live up to their promise on high Q factors, and to verify if they are useful for use with torsion pendulums, with a special focus on TOBA. The experiments here also provide a basic setup for the usage of crystalline fibres in the use of torsion pendulums, and provide a quantitative idea of their usefulness in precision experiments. A common problem in Q factor experiments is the difficulty of separating the intrinsic Q of the sample with the loss from the setup. Of cause, this problem is faced here as well. On the other hand, as our setup is that of a torsion pendulum, we can say with confidence that the values achieved here will be achievable with a similar setup, which will be very useful as we adapt it for use with TOBA. In a sense, these experiments are also experiments in clamp design and setups, and not simply measurements of intrinsic values.

Chapter 2

The Torsion Pendulum

The basic theory behind the humble torsion pendulum is as follows. Restoring torque is generated by the suspension fibre as it is twisted. The nature of this torque originates from the mechanics of materials, and is derived below. The following derivation assumes a suspension by a single fibre.

The shear stress at any point inside the fibre τ_s, is related to the strain angle γ via the shear modulus μ as follows:

$$\tau_s = \mu\gamma. \tag{2.1}$$

As an aside, the shear modulus μ is related to the more famous Young's modulus Y and Poisson's ratio ν via the relation

$$\mu = \frac{Y}{2\,(1+\nu)}, \tag{2.2}$$

with the assumptions of a isotropic and homogeneous material.

We now note that the strain angle is related to the angle of twist of the fibre θ, with

$$\gamma = r\frac{\theta}{L}, \tag{2.3}$$

with r being the distance away from the centre of the fibre, and L being the length of the fibre. This relation is a geometric one, assuming that the twist that occurs is linear, which would be reasonable for a homogeneous material undergoing a small twist.

By relating the two equations, we obtain

$$\tau_s = \mu r\frac{\theta}{L}. \tag{2.4}$$

The moment (torque) M generated by the fibre can then be calculated by via the integration over the cross sectional area A, leading to

$$\begin{aligned} M &= -\int_0^R \tau_s r dA \\ &= -\mu\frac{\theta}{L}\int_0^R r^2 dA \\ &= -\mu\frac{\theta}{L}J, \end{aligned} \tag{2.5}$$

with R being the radius of the fibre, and the identification of J as the second moment of area. The negative sign comes from the recognition that the torque generated is in the opposite direction from the angle of twist.

The second moment of area for the geometry of fibre, i.e. an cylinder, is given by

$$\begin{aligned} J &= \int_0^R r^2 dA \\ &= \int_0^R r^2 d(\pi r^2) \\ &= \int_0^R 2\pi r^3 dr \\ &= \frac{\pi R^4}{2} = \frac{\pi D^4}{32}, \end{aligned} \tag{2.6}$$

with D the diameter of the fibre.

We can now identify the torsional constant, by relating (2.5) to an angular version of Hook's law,

$$M = -\kappa\theta, \tag{2.7}$$

giving

$$\begin{aligned} \kappa &= \frac{\mu J}{L} \\ &= \frac{\mu}{L}\frac{\pi R^4}{2} = \frac{\mu}{L}\frac{\pi D^4}{32}. \end{aligned} \tag{2.8}$$

Starting from the relation between torque and angular acceleration for a body with a fixed moment of inertia I,

$$M = I\ddot{\theta}, \tag{2.9}$$

which combined with Hook's law gives

$$I\ddot{\theta} = -\kappa\theta, \tag{2.10}$$

which we identify as simple harmonic motion, giving an angular resonance frequency ω_0 of

$$\omega_0 = \sqrt{\frac{\kappa}{I}}, \tag{2.11}$$

with κ identified above and $I = \int r^2 dm$ depending on the geometry of the pendulum, with

$$I = \frac{1}{12}ml^2 \tag{2.12}$$

for a thin rod, and

$$I = \frac{1}{2}mr^2 \tag{2.13}$$

for a solid disc.

This completes the basic theory behind torsion pendulums. In practice, there are many complicating factors, which have been subjected to research over the years, such as dissipation (which leads to thermal noise, which we will discuss in detail in this work), the the actual resonance frequency would differ, due to many complicating factors, such as anisotropy in the fibre, etc.

2.1 Torsion-Bar Antenna (TOBA)

The recent direct detections of gravitational waves, starting from GW150914 [12] has brought forth a new era of astronomy. By these detections of black holes, we have discovered a population of black holes that were previously unknown to mankind. Unfortunately, the current ground based interferometric based detectors such as aLIGO, AdVirgo and KAGRA, are limited in the range of frequencies in which they can detect gravitational waves [13]. The given sensitivity curves for these detectors are generally given from 10 Hz to 7000 Hz.

As mentioned in the introduction, TOBA is a proposed gravitational wave detector [4] that uses a torsion pendulum in its design. As compared to standard ground based interferometric based detectors, it targets a lower frequency band, that of 0.1 Hz to 10 Hz. The two perpendicular bars spanning the horizontal plane that make up TOBA will nominally be 10 m long, suspended by a fibre from their centre of mass. When gravitational waves pass though, tidal forces from the waves will cause angular movement, which will be measured with a sensor. There are already sub-meter scale prototypes of TOBA already demonstrating proof of concept and setting bounds on the gravitational wave stochastic background in the band of interest [14].

Pendulum based detectors have a resonance frequency of $\omega_0 = \sqrt{\frac{g}{L}}$, with g being fixed due to the detectors being located on Earth, L has a practical range of up to the order of 10 m, leading to resonance generally being between 0.1 Hz to 10 Hz. This sets the lowest frequency in which these detectors can be accurate. Of cause, space based detectors, not being subjected to the Earth's gravitational field, do not have this limit, and indeed, both LISA and DECIGO targets a lower frequency band [15, 16]. Obviously, space based detectors, being free from Earth bound constrains, can achieve a much better sensitivity than TOBA. On the other hand, a much lower cost and much greater accessibility means that it is complimentary to space based detectors, not unlike the situation with earth based telescopes and the Hubble space telescope.

Other uses for TOBA would be for an early warning system for earthquakes [17], and by the same token, an early warning system for tsunamis as well. It can also be used to measure gravity gradient noise — noise generated by moving Newtonian noise sources. Essentially, changing positions of masses nearby would cause their Newtonian gravitational force to change with respect to the detector, generating noise[1].

TOBA targets the range in between LISA and aLIGO, and can thus observe intermediate mass black holes mergers, with the frequency of this allowing us to test super massive black hole formation theories. At the target sensitivity, with a signal to noise ratio of 5, it will have an observation range of 10 Gpc for black hole binary mergers with a total mass of 10^5 solar masses [4].

The targeted Q is that of $Q \gtrsim 10^8$, which is required to ensure that thermal noise is not a limiting factor in the final TOBA [4].

[1] Technically, these also generate gravitational waves, but are many orders smaller in magnitude that we do not even need to give them even a moment of consideration.

2.2 Measurement of G

The universal gravitational constant, G is one of the least precise physical constants known to mankind [18]. This is not for lack of trying, but rather due to the nature of gravity, which unlike other forces, cannot be shielded from, and there is a rather strong gravitational field on Earth that all gravitational experiments have to contend with. The torsion pendulum, with its degree of freedom being orthogonal to Earth's gravity, is a natural choice for such experiments. The celebrated use by Henry Cavendish for the measurement of the mean density of the Earth [1], now more commonly interpreted in terms of G, is one of the earliest recorded uses of the torsion pendulum for precision measurements.

One of the most popular method utilising torsion pendulums to measure G is via something known as the time of swing. This method has been used over the years [19, 20], and is still popular to this day [3, 21]. One of the biggest issues preventing further accuracy of this method is known as the Kuroda bias [22], which suggests that the results is biased by the anelasticity of the fibre, which will be smaller as Q increases. To this end, the use of cryogenic systems have been deployed [3, 23], and fused silica has been used [21].

Chapter 3

Thermal Noise

The nature of mechanical systems is that thermal noise becomes a limit of sensitivity in measurements. This occurs to every system, from the basic spring block system to the intricate systems of the mechanical watch. Simply put, thermal energy leads to vibration, and thus noise.

3.1 The Fluctuation-Dissipation Theorem

The fluctuation-dissipation theorem gives us an understanding of how thermal noise affects a system. It essentially states that in the same way that a system loses "useful" energy via dissipative mechanisms which turns into thermal energy, thermal noise is generated by the same route, in which thermal energy turns into noise via the opposite direction. This was first formulated by Harry Nyquist in the context of Johnson noise in circuits [24], but was generalised in 1951 by Herbert B. Callen and Theodore A. Welton [25]. It quantitatively links the linear response to external forces to the fluctuations arising from thermodynamic equilibrium. This link between dissipative systems and spontaneous fluctuations was shown to have much flexibility, reproducing results from Brownian motion, the Plank radiation law among other effects.

The theorem is given by

$$\langle F^2 \rangle = \frac{2}{\pi} \int_0^\infty \Re(Z(\omega)) E(\omega, T) d\omega, \tag{3.1}$$

with $\langle F^2 \rangle$ being the mean square of a generalised force, $\Re(Z(\omega))$ being the real part of a generalised impedance and with the energy $E(\omega, T)$ being

$$E(\omega, T) = \frac{1}{2}\hbar\omega + \hbar\omega(e^{\frac{\hbar\omega}{k_B T}} - 1)^{-1}, \tag{3.2}$$

the mean energy of an oscillator of angular frequency ω at temperature T.

At high temperatures ($k_B T \gg \hbar\omega$), this simplifies to

$$E(\omega, T) \simeq \frac{1}{2}\hbar\omega + \hbar\omega(1 + \frac{\hbar\omega}{k_B T} - 1)^{-1} \simeq k_B T, \tag{3.3}$$

which matches the result from equipartition theory, giving

$$\langle F^2 \rangle = \frac{2}{\pi} k_B T \int_0^\infty \Re(Z(\omega)) d\omega, \tag{3.4}$$

or the more familiar form

$$\langle F^2 \rangle df = 4 k_B T \Re(Z(f)) df, \tag{3.5}$$

where $2\pi f = \omega$ and $\langle V^2 \rangle df$ is the mean square of the force within the frequency interval df. If we then let F be voltage and remember that the real part of impedance is resistance, we recover the Nyquist relation.

If we are interested in the displacement of the system, we note that in frequency space, $x = \frac{\dot{x}}{i\omega}$ and $x = -\frac{\ddot{x}}{\omega^2}$. Furthermore, we also note that the impedance is defined by

$$F = Z(\omega)\dot{x}, \tag{3.6}$$

where $\dot{x}$ would be the generalised velocity, giving the velocity version of the fluctuation-dissipation theorem to be

$$\langle \dot{x}^2 \rangle = \frac{4 k_B T \Re(Z(\omega))}{|Z(\omega)|^2} = 4 k_B T \Re(Y(\omega)), \tag{3.7}$$

and the displacement version would be

$$\langle x^2 \rangle = \frac{4 k_B T}{\omega^2} \Re(Y(\omega)), \tag{3.8}$$

with the admittance defined by $Y = \frac{1}{Z}$. This is the thermal noise spectrum for a generic system.

3.2 Q Factor

The Q factor, also known as the quality factor, is a dimensionless parameter, that characterises how underdamped a system at resonance is. The higher the Q factor, the longer a system will oscillate. It is usually defined[1] by the resonance frequency f_0 divided by the full width half maximum of the resonance peak in frequency space Δf (with the peak measured in energy),

$$Q = \frac{f_0}{\Delta f}. \tag{3.9}$$

The Q factor in general is dependent on the frequency, but in practice is rather insensitive over a rather large range of frequencies [7, 27]. In the case of torsion pendulums, there is also a dependence on amplitude [23, 28], among other possible properties.

We point out here that you can get Q from the thermal noise spectrum, as resonance also occurs there, as will be shown later.

3.2.1 Viscous Damping

There are two simplified models of damping, that of viscous damping and structural damping. Viscous damping is damping that is proportional to the velocity of the system, giving a damped harmonic oscillator equation of motion

$$F = m\ddot{x} + b\dot{x} + kx, \tag{3.10}$$

with b being the damping coefficient. This type of damping is also known as classical damping, because it is the most studied form of damping (analytically), even if most real life damping do not correspond exactly to it.

We justify using the harmonic oscillator by pointing out that for it is a good approximation to most potential wells, especially if kept to small perturbations.

To link the Q factor and the fluctuation dissipation theorem, we first start out with applying the fluctuation dissipation on this system.

The admittance is then

[1] Q was initially coined by K.S. Johnson in 1920 as the ratio of reactance to effective resistance in a coil or capacitor, and the story of how it evolved to its current day definition is chronicled in [26].

$$\begin{aligned} Y(\omega) &= \frac{1}{Z(\omega)} \\ &= \frac{\dot{x}}{F} \\ &= \frac{1}{i\omega m + b + \frac{k}{i\omega}} \\ &= \frac{1}{b + i(\omega m - \frac{k}{\omega})}, \end{aligned} \tag{3.11}$$

where we use the fact that in frequency space,

$$i\omega x = \dot{x} \tag{3.12}$$

and

$$i\omega \dot{x} = \ddot{x}. \tag{3.13}$$

The real part of the admittance is

$$\begin{aligned} \Re\left(Y(\omega)\right) &= \Re\left(\frac{1}{b + i\left(\omega m - \frac{k}{\omega}\right)}\right) \\ &= \frac{b}{b^2 + \left(\omega m - \frac{k}{\omega}\right)^2} \end{aligned} \tag{3.14}$$

Then applying the fluctuation-dissipation theorem, we now have

$$\begin{aligned} \langle x^2 \rangle &= \frac{4k_B T}{\omega^2} \Re\left(Y(\omega)\right) \\ &= \frac{4k_B T}{\omega^2} \frac{b}{b^2 + \left(\omega m - \frac{k}{\omega}\right)^2}. \end{aligned} \tag{3.15}$$

Solving for the maximum, we find out that it occurs at

$$\omega_0 = \frac{\sqrt{-b^2 + 2mk}}{\sqrt{2}m}, \tag{3.16}$$

and in the case of $b^2 \ll mk$,

$$\omega_0 \simeq \sqrt{\frac{k}{m}}, \tag{3.17}$$

where the slightly damped case has the same resonance frequency as the simple harmonic oscillator, as we expect it to be.

In order to obtain the Q factor, we now need the full width half maximum (FWHM), meaning the difference in the solutions to

$$\frac{1}{2}\frac{4k_BT}{\omega_0^2}\frac{b}{b^2+\left(\omega_0 m-\frac{k}{\omega_0}\right)^2}=\frac{4k_BT}{\omega^2}\frac{b}{b^2+\left(\omega m-\frac{k}{\omega}\right)^2}. \tag{3.18}$$

The solutions are

$$\omega_+=\frac{\sqrt{\frac{\sqrt{-b^2m^4(b^2-4km)}}{m^4}-\frac{b^2}{m^2}+\frac{2k}{m}}}{\sqrt{2}} \tag{3.19}$$

and

$$\omega_-=\frac{\sqrt{-\frac{\sqrt{-b^2m^4(b^2-4km)}}{m^4}-\frac{b^2}{m^2}+\frac{2k}{m}}}{\sqrt{2}} \tag{3.20}$$

with ω_+ and ω_- referring to the larger and smaller solutions respectively.

The difference is then

$$\frac{\sqrt{\sqrt{b^2m^4\left(4km-b^2\right)}-b^2m^2+2km^3}-\sqrt{-\sqrt{b^2m^4\left(4km-b^2\right)}-b^2m^2+2km^3}}{\sqrt{2}m^2}\simeq\frac{b}{m}, \tag{3.21}$$

where we assume again that $b^2\ll mk$ and only deal with first order in b.

We thus end up with a Q factor of

$$Q\simeq\frac{\omega_0 m}{b}, \tag{3.22}$$

which becomes accurate for large Q.

We have now derived Q using the fluctuation dissipation theorem, for a system with viscous damping.

Rewriting the fluctuation dissipation theorem in terms of Q, we have, for the case of $\omega\ll\omega_0$,

$$\begin{aligned}\langle x^2\rangle&=\frac{4k_BT}{\omega^2}\frac{b}{b^2+\left(\omega m-\frac{k}{\omega}\right)^2}\\&\simeq\frac{4k_BTb}{k^2}=\frac{4k_BT\omega_0 m}{k^2Q},\end{aligned} \tag{3.23}$$

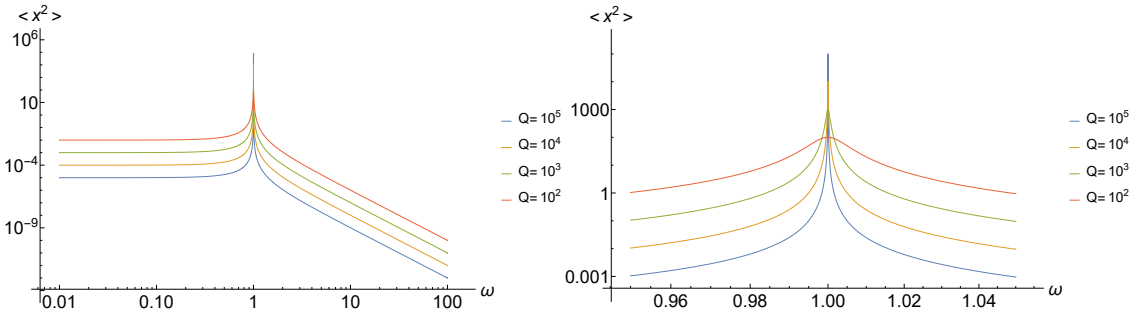

(A) Q from bottom: 1×10^5,1×10^4,1×10^3, and 1×10^2

(B) Same graph as left, but zoomed in to show the peaking at the resonance frequency

FIGURE 3.1: Loglog plots of the thermal noise spectrum of various viscous damped system with parameters $k = 1$ and $m = 1$, leading to resonance at $\omega = 1$ with various Q factors. The higher the Q, the higher the response at resonance, and lower everywhere else. Both TOBA and second generation ground based gravitational wave detectors have an operating sensitivity to the right of the suspension's resonance, where thermal noise is low.

and for the case of $\omega \gg \omega_0$,

$$\langle x^2 \rangle \simeq \frac{4k_B T b}{\omega^4 m^2} = \frac{4k_B T \omega_0}{\omega^4 m Q}. \tag{3.24}$$

This leads us to the understanding that at frequencies far away from resonance, with everything else being equal, a higher Q leads to lower thermal noise. The corollary to this is that at frequencies near resonance, noises are amplified drastically, with

$$\langle x^2 \rangle \simeq \frac{4k_B T}{\omega_0^2 b} = \frac{4k_B T Q}{\omega_0^3 m} \tag{3.25}$$

at $\omega \simeq \omega_0$.

The utility of Q comes from it being a measurable quantity, especially at resonance.

In a significantly underdamped oscillator, the response is known to be

$$x = e^{-\frac{b}{2m}t} a \cos(\omega_0 t), \tag{3.26}$$

and the time independent part of the exponent can be rewritten as

$$\frac{b}{2m} = \frac{\omega_0}{2Q}, \tag{3.27}$$

which means that we can calculate the Q from the decay envelop and the resonance frequency in practice, with the equation

$$Q = \frac{\tau\omega_0}{2} = \pi\tau f_0, \tag{3.28}$$

where τ is the time constant of the decay envelop and given by $\tau = \frac{2m}{b}$. This, as we will see later, is essential in experimental measurements of Q.

3.2.2 Structural Damping

Now, if we consider structural damping, which is modelled by

$$F = m\ddot{x} + k(1 + i\phi)x, \tag{3.29}$$

where ϕ is known as the loss angle.

This is a generalised version of Hook's law, where the restoring force is not instantaneous, but out of phase by the loss angle ϕ.

As can be inferred from its name, the loss angle is linked to the amount of energy dissipated out of the system.

To apply the fluctuation-dissipation theorem to this model, we repeat ourselves by first calculating the admittance,

$$\begin{aligned} Y(\omega) &= \frac{1}{Z(\omega)} \\ &= \frac{\dot{x}}{F} \\ &= \frac{1}{i\omega m + \frac{k(1+i\phi)}{i\omega}} \\ &= \frac{1}{\frac{k\phi}{\omega} + i\left(\omega m - \frac{k}{\omega}\right)}, \end{aligned} \tag{3.30}$$

and then calculating the real part of it,

$$\Re\left(Y(\omega)\right) = \frac{\frac{k\phi}{\omega}}{\left(\frac{k\phi}{\omega}\right)^2 + \left(\omega m - \frac{k}{\omega}\right)^2}. \tag{3.31}$$

We now have

$$\begin{aligned} \langle x^2 \rangle &= \frac{4k_BT}{\omega^2}\Re\left(Y(\omega)\right) \\ &= \frac{4k_BT}{\omega^2}\frac{\frac{k\phi}{\omega}}{\left(\frac{k\phi}{\omega}\right)^2 + \left(\omega m - \frac{k}{\omega}\right)^2}. \end{aligned} \tag{3.32}$$

Assuming a constant[2] ϕ, we solve for the maximum, which happens with a frequency of

$$\omega_0 = \sqrt{\frac{3km + \sqrt{k^2m^2(4-5\phi^2)}}{5m^2}}, \tag{3.33}$$

and as we have come to expect,

$$\omega_0 \simeq \sqrt{\frac{k}{m}}, \tag{3.34}$$

in the case of $\phi^2 \ll 1$.

We now note that the mean fluctuation equations (3.15) and (3.32) differ only by the replacement of $b \to \frac{k\phi}{\omega}$. This means that the FWHM can be approximated (to first order) by

$$\frac{b}{m} \to \frac{k\phi}{\omega_0 m} = \omega_0\phi, \tag{3.35}$$

where the usage of ω_0 is justified by noting that the FWHM is small with respect to the magnitude of ω_0, and thus approximately constant over the range in question.

This leads us to the conclusion that for structural damping, the relationship between the Q factor and the loss angle is exceedingly simple, and given by

$$Q = \frac{1}{\phi}, \tag{3.36}$$

with the oft repeated caveat that it only holds true for large Q.

Rewriting the fluctuation dissipation theorem in terms of Q, we have, for the case of $\omega \ll \omega_0$,

$$\begin{aligned}\langle x^2\rangle &= \frac{4k_BT}{\omega^2}\frac{\frac{k\phi}{\omega}}{\left(\frac{k\phi}{\omega}\right)^2 + \left(\omega m - \frac{k}{\omega}\right)^2} \\ &\simeq \frac{4k_BT\phi}{k\omega(\phi^2+1)} \simeq \frac{4k_BT}{k\omega Q},\end{aligned} \tag{3.37}$$

while for the case of $\omega \gg \omega_0$,

$$\langle x^2\rangle \simeq \frac{4k_BTk\phi}{\omega^5m^2} = \frac{4k_BTk}{\omega^5m^2Q}. \tag{3.38}$$

[2]Technically another maximum occurs at 0 Hz with a constant ϕ, so what we mean is a constant ϕ over the range that we do care about, similar to white noise, where a similar infinite energy problem appears if you blindly apply the concept over all frequencies. To be specific, as ω tends to zero, it means that that the time lag for the restoring force tends to infinity, which is patently unphysical. In [29], it is pointed out that this term needs to be an odd function of frequency, i.e. be zero at 0 Hz. The same article also goes into detail why this divergence is not a practical issue for real systems, and is worth a read.

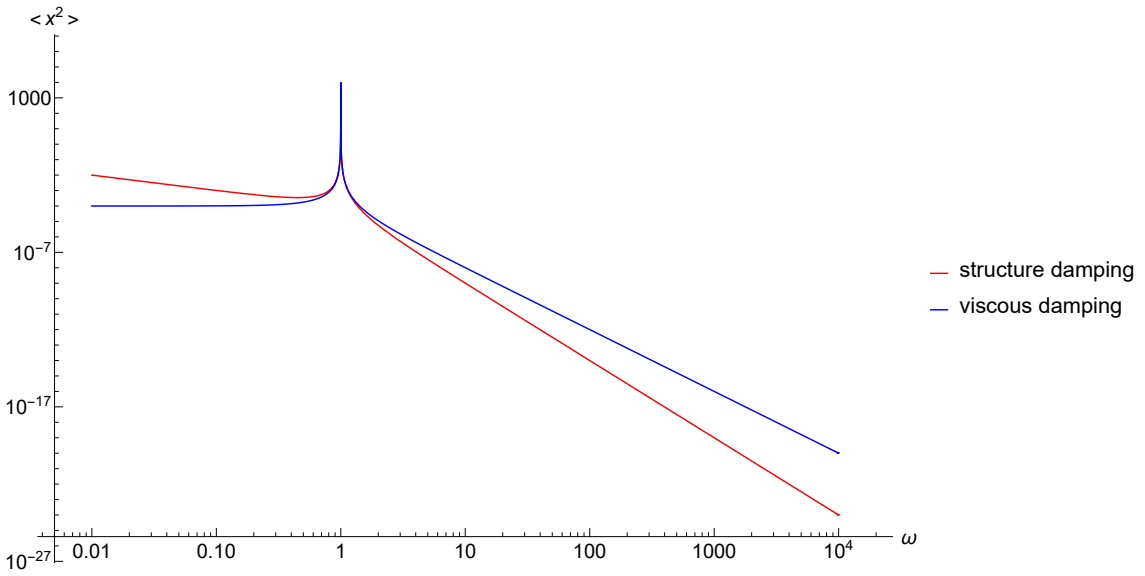

FIGURE 3.2: loglog plot of thermal fluctuation spectrums of (blue) viscous damping and (red) structural damping, illustrating the different behaviour at frequencies away from resonance. Parameters are $Q = 10^4$, with $\omega_0 = 1$. Of particular interest is the ω^{-5} dependence in the structural case versus the ω^{-4} dependence in the viscous case at frequencies larger than resonance. Of cause, in reality, the loss factor for structural damping is not a real constant with respect to frequencies, but it generally is stable within a band of an order of magnitude across many orders of magnitude of frequencies [30], and thus the overall trend does hold.

Yet again, it peaks at resonance at $\omega \simeq \omega_0$, with

$$\langle x^2 \rangle \simeq \frac{4k_B T}{\omega_0 k \phi} = \frac{4k_B T Q}{\omega_0 k}. \tag{3.39}$$

We now justify our earlier assumption of a constant loss angle by pointing out again that literature has shown that the loss angle is (somewhat) independent of frequency, at least for a large variety of materials, over a large range of frequencies [27]. There is, however, some evidence that there is some frequency dependence, at least for some configurations.

We note here that as a result of structure based damping, the thermal noise falls of faster with respect to frequencies at frequencies higher than resonance.

In any case, given how similar structural damping behaves as compared to viscous damping at resonance, the relation between the ringdown and Q holds true here too.

3.2.3 An Intuitive Definition of Q

A different way to define Q is by relating it to the energy stored in a system and the energy dissipated in one cycle at resonance. Specifically, it is given by

$$Q = 2\pi \frac{E}{\Delta E}, \tag{3.40}$$

where E is the energy stored in the system and ΔE is the energy loss by one cycle of the system.

We will see how this is equivalent to the initial definition, at least in the context of high Q, by using eq. 3.26.

Consider that the energy of a system is proportional to the square of the amplitude of the generallised amplitude (think spring block). We then have the ratio $\frac{E}{\Delta E}$ for one cycle (using eq. 3.26) given by

$$\begin{aligned} \frac{E}{\Delta E} &= \frac{1^2}{1^2 - \left(e^{-\frac{b}{2m}\frac{1}{f_0}}\right)^2} \\ &= \frac{1}{1 - e^{-\frac{b}{mf_0}}} \\ &\simeq \frac{1}{1 - 1 + \frac{b}{mf_0}} \\ &= \frac{mf_0}{b}, \end{aligned} \tag{3.41}$$

where the approximation is justified as $b^2 \ll mk$ (high Q) is equivalent to $\frac{b}{mf_0} \ll 1$.

By referencing eq. 3.22 ,$Q \simeq \frac{\omega_0 m}{b}$, we see that eq. 3.40 is consistent with previous definitions of Q. We justify the extension to systems with structural damping by pointing out that a system at resonance is only moving at f_0, and thus the argument will hold with the replacement $b \to \frac{k\phi}{\omega_0}$.

This is a more physical intuitive definition of Q, and easier to keep in mind as the motivation for the experiments that follow.

3.3 Thermal Noise for Torsion Pendulums

Now, we can apply this knowledge to torsion pendulums. We shall focus our attentions onto structural damping, where the thermal fluctuation spectrum of eqn 3.32 becomes

$$\langle\theta^2\rangle = \frac{4k_BT}{\omega^2}\frac{\frac{k\phi}{\omega}}{\left(\frac{\kappa\phi}{\omega}\right)^2 + \left(\omega I - \frac{\kappa}{\omega}\right)^2}, \tag{3.42}$$

with the simple replacement of $m \to I$ and $k \to \kappa$.

For the case of $\omega \gg \omega_0$,

$$\langle\theta^2\rangle \simeq \frac{4k_BT\kappa}{\omega^5 I^2 Q} = \frac{k_BT\mu\pi D^4}{8\omega^5 I^2 LQ}, \tag{3.43}$$

where eqn 2.8 was brought in.

This signifies that with all else being equal, the fibre used should be as long as possible, Q as high as possible, and D as small as possible, with the dependence on D being a staggering fourth power. This explains the popularity of tungsten for the use in torsion pendulum experiments, due to its high tensile strength, leading to a smaller diameter required.

If we assume a fixed weight mg to carry along with a fixed safety factor s, the minimum diameter will be related to the tensile strength S_t by

$$smg = S_t\pi\frac{D^2}{4}, \tag{3.44}$$

leading to

$$\langle\theta^2\rangle \simeq \frac{m^2}{I^2}\frac{2k_BT\mu s^2 g^2}{\omega^5 L {S_t}^2 \pi Q}. \tag{3.45}$$

Chapter 4

Material Selection, Experimental Concerns

4.1 The Quest for High Q

Seeing that Q is one of the free parameters in the thermal noise spectrum, the hunt for high Q begin. Another reason to study high mechanical Q materials in the gravitational wave community was for use in Weber bars [31–33], which required a high Q for resonance with passing gravitational waves. This was a big motivation behind bulk Q measurements.

4.1.1 Bulk Q

These resonant mass detectors (Weber bars) utilised the fact that the high Q is, the larger the resonance becomes. Aluminium alloy 5056 was given much attention, due to studies finding it to be the aluminium alloy with the highest Q at 4 K [34], with detectors built all over the globe. These detectors were large, usually weighting over a ton. Selected bulk Q measurements are summarised in table 4.1, which showcases how bulk Q changes with temperature, and the gap between metals and crystals. Weber bars were not build with crystals, as current technology does not allow for fabrication of large crystals weighting over a ton.

4.1.2 Fibre Q

While table 4.1 showcases the bulk Q, measured Q in fibres have historically been quite a little lower. For simplicity, flat cantilevers will also count as fibres for the purposes of this work. Effects such as thermoelastic loss, surface loss, clamp loss and recoil loss conspire

TABLE 4.1: Table of bulk Q for various materials, from metals to amorphous fused silica to single crystals. The asterisk next to fused silica and quartz indicates data taken from fibres or cantilevers, rather than a bulk resonator. Data taken from [5–8, 10, 34–39]. There are many other works on bulk Q, with many works showing results orders of magnitude smaller. In general, these results are very dependent on annealing and surface properties, along with the experimental setup. Note that lower temperatures generally lead to higher Q, with fused silica being an exception. The cryogenic value of Q for sapphire [10] is actually the current world record in the literature for mechanical Q.

Material	300K	4 K	50 mK
Aluminium 5056	3×10^5	4×10^7	6.5×10^7
Copper Beryllium	3×10^5	3×10^6	7.8×10^6
Niobium	1×10^6	2×10^7	4.2×10^7
Molybdenum	3×10^5	2×10^7	4.4×10^7
Tungsten	2×10^5	9×10^6	1.2×10^7
Fused Silica*	2×10^8	2×10^3	
Quartz*	5×10^6	7×10^7	
Sapphire (Al_2O_3)	2.6×10^8	5×10^9	
Silicon	9×10^7	2×10^9	

TABLE 4.2: High torsion Q values of torsion pendulums, taken from literature. From left, values taken from [3],[3],[23],[41], and [42]. The torsion pendulum in [42] does not have a uniform fibre thickness. Note that all of them fall short of the requirement for TOBA of $Q \gtrsim 10^8$. In this work, torsion measurements of bulk resonators are counted as bulk Q measurements, due to the aspect ratio of the resonators.

Material	CuBe	AL5056	Sapphire	Silica	Silica
Torsional Q	$\mathbf{1.2 \times 10^5}$	$\mathbf{1.6 \times 10^5}$	$\mathbf{\sim 10^6}$	$\mathbf{\sim 10^6}$	$\mathbf{7 \times 10^6}$
Temperature	~4 K	~4 K	4.2 K	300 K	300 K
Thickness	20 µm	25 µm	???	70 µm	150~500 µm

to reduce the measured Q. The details of these effects will be detailed later, but suffice to say that Q measurements is harder with fibres than with bulk. Most fibre measurements are done via clamped-free samples, i.e. a fibre clamped at one end. The highest fibre Q value is in table 4.1, and a good reference to various fibre Q can be found in [30].

4.1.3 Torsion Q in Fibres

The current literature on high Q torsion pendulums is summarised in table 4.2. We see that similar to fibre measurements, the highest value belongs to fused silica. Metal wires used at room temperature for G measurements typically have a value of $\sim 10^3$ [28, 40]

4.2 Crystal Fibres and Torsion Pendulums

In this work, we focus on the measurement of crystal fibres, especially sapphire. Crystals have been shown in literature to have high intrinsic Q [7, 8], with about two to three orders of magnitude higher than that of metals, which typically reach 10^5. See Table 4.1 for details. Given the requirement for TOBA, in which suspension thermal noise does not become a limiting noise source, the only reasonable choice is to consider crystalline fibres. If we refer back to 3.43, we note that the tensile strength for crystalline materials depend drastically on their finish, with a high quality surface providing a higher tensile strength than metals, even that of tungsten and piano wire [43, 44]. On the flip side, poor surface quality will lead to over an order of magnitude decrease in tensile strength. With a higher tensile strength, higher Q, and similar Young and shear moduli compared to metals, crystalline materials are the best choice to lower thermal noise in both pendulums and torsion pendulums.

This was first implemented for gravitational wave detectors by GEO 600 (fused silica) [45], and has since applied to aLIGO (fused silica fibres), KAGRA (sapphire fibres) and AdVirgo (fused silica fibres). However, these are pendulum systems, and not torsion pendulums. Research on torsion pendulums using crystalline wires is scarce, with the only known data (in my knowledge) for sapphire, coming from [23], in a graph, at 4.2 K no less, showing the dependence of Q factor with amplitude. Unfortunately, no other data is provided in this graph, with the details behind the experiment unknown. Although the graph showed that sapphire provided the highest Q factor among the materials tested, with a value on the order of 10^6, it is firstly technically insufficient for the use in TOBA and secondly has a severe lack of details on the experiment. For example, details like which crystal axis was the sapphire tested on as well as the dimensions of the sapphire used are completely unknown.

On the other hand, there is more information on silica, with $Q = 7.4 \times 10^5$ for a torsion pendulum to study the free fall mode of LISA [46], $Q \sim 5 \times 10^4$, for a torsion pendulum used to measure G [21] and $Q = 7 \times 10^6$ for a torsion pendulum used to study the viability of silica fibres as the suspension for gravitational wave detectors [42].

Unfortunately, silica is known to be not suitable for cryogenic cooling, with the quality factor falling to below metals [38] at cryogenic temperatures. This is the reason why sapphire is being used in KAGRA and sillicon is being studied for possible use in 3rd generation gravitational wave detectors. With the selection of sapphire as a material

TABLE 4.3: Measurements of sapphire Q over the years. From top: [10], [8], [47], [7], [48], [23], [49], and [30]. We can see that at room temperatures, flexural modes are limited by thermoelastic damping. Note the lack of data on low frequency torsion, which would be the quantity of interest for torsion pendulums.

highest Q	Q type	Frequency	Temperature
$\mathbf{5 \times 10^9}$	Bulk	30000 Hz	4 K
$\mathbf{2.7 \times 10^8}$	Bulk	53591 Hz	300 K
$\mathbf{2.5 \times 10^8}$	Bulk	67759 Hz	4 K
$\mathbf{6.4 \times 10^7}$	Bulk	73977 Hz	300 K
$\mathbf{1.1 \times 10^7}$	Flexural	199 Hz	6 K
$\mathbf{\sim 10^6}$	Torsion	???	4 K
$\mathbf{\sim 5 \times 10^4}$	Flexural	~20 Hz	300 K
$\mathbf{\sim 10^4}$	Flexural	~8 Hz	300 K

to study, we first must look at past measurements of sapphire, tabulated in Table 4.3. Sapphire has the current world record for the highest ever measured mechanical Q of 5×10^9 [10], and even has a room temperature value of 2.7×10^8 [8].

Despite these limitations, this provides motivation to work with crystal fibres, as it provides evidence that even for torsional modes, they surpass metal wires in terms of Q.

4.3 Surface Loss and Q

There is a growing body of evidence that high Q measurements of fibres are almost always limited by surface loss. In this case, we distinguish fibres from simple bulk measurements where the samples have dimensions that are of the same order with each other. Surface losses are caused by the surface being damaged compared, with the bulk, with absorbed molecules, irregularities leading to a lower Q then the bulk.

This can be seen clearly in [50], where a fused silica sample had its Q factor falling by a factor of four just from hitting against a copper rod. [51] shows a clear trend between size and thus energy stored by surface to volume ratio for silicon, and similar relations have been shown for fused silica [41, 52, 53]. This relation has been shown even on the nano scale, with [54] having nanometre silicon wires following the same trend.

There is a simplified model which we can use to quantify the loss from the surface. The effective Q depends on not just the Q of the bulk, but also of any other energy dissipation mechanism. The effective Q is thus also related to the Q of the other mechanisms, but not directly, as the amount of energy loss though other mechanisms is related to the amount

of energy stored in them. Using the alternate definition of Q is given by $Q = 2\pi\frac{E}{\Delta E}$ (eq. 3.40), we can see that

$$Q_{eff} = 2\pi\frac{E_1 + E_2 + ...}{\Delta E_1 + \Delta E_2 + ...}, \tag{4.1}$$

where E_1 and E_2 represents the energy from the various mechanisms.

Limiting our discussion to bulk and surface loss, we can rewrite this equation as

$$\frac{1}{Q_{eff}} = \frac{1}{2\pi}\frac{\Delta E_{bulk} + \Delta E_{surface}}{E_{bulk} + E_{surface}}. \tag{4.2}$$

We now assume that the energy stored in the surface is insignificant compared to what is stored in the bulk,$E_{bulk} \gg E_{surface}$, giving

$$\begin{aligned}\frac{1}{Q_{eff}} &\simeq \frac{1}{2\pi}\frac{\Delta E_{bulk} + \Delta E_{surface}}{E_{bulk}} \\ &= \frac{1}{Q_{bulk}} + \frac{1}{2\pi}\frac{\Delta E_{surface}}{E_{bulk}} \\ &= \frac{1}{Q_{bulk}} + \frac{1}{2\pi}\frac{\Delta E_{surface}}{E_{surface}}\frac{E_{surface}}{E_{bulk}} \\ &= \frac{1}{Q_{bulk}} + \frac{1}{Q_{surface}}\frac{E_{surface}}{E_{bulk}}.\end{aligned} \tag{4.3}$$

Now, if we further assume that the surface layer has a characteristic thickness h in which $Q_{surface}$ exists, which in other words means a damaged layer with a (presumably) lower Q, we can rewrite the term $\frac{E_{surface}}{E_{bulk}}$ as $h\frac{\int_S \epsilon^2 dS}{\int_V \epsilon^2 dV}$, where we recall that the potential energy per unit volume is given by $\frac{1}{2}Y\epsilon^2$ for a simple strain, and use a further approximation that the surface layer has the same Young's modulus as the bulk.

The realised Q of a sample can then be approximated by the following equation for a simple strain,

$$\frac{1}{Q_{eff}} \sim \frac{1}{Q_{bulk}} + \frac{1}{Q_{surface}}h\frac{\int_S \epsilon^2 dS}{\int_V \epsilon^2 dV}. \tag{4.4}$$

In the case of torsion, the term $\frac{\int_S \epsilon^2 dS}{\int_V \epsilon^2 dV}$ is replaced as we note that the energy stored per unit volume via shear is given by $\frac{1}{2}\mu\gamma^2$, leading to the effective Q for samples with pure shear to be

$$\frac{1}{Q_{eff}} \sim \frac{1}{Q_{bulk}} + \frac{1}{Q_{surface}}h\frac{\int_S \gamma^2 dS}{\int_V \gamma^2 dV}, \tag{4.5}$$

where we once again assume the same shear modulus for both the surface and the bulk.

With respect to torsion pendulums, we evaluate

$$\begin{aligned}\frac{\int_S \gamma^2 dS}{\int_V \gamma^2 dV} &= \frac{\int_S \left(\frac{R\theta}{L}\right)^2 dS}{\int_V \left(\frac{r\theta}{L}\right)^2 dV} \\ &= \frac{\int_0^L \left(\frac{R\theta}{L}\right)^2 2\pi R dl}{\int_0^L \int_0^R \left(\frac{r\theta}{L}\right)^2 2\pi r dr dl} \\ &= \frac{\left(\frac{\theta}{L}\right)^2 2\pi R^3 L}{\left(\frac{\theta}{L}\right)^2 2\pi \frac{R^4}{4} L} \\ &= \frac{4}{R} = \frac{8}{D}. \end{aligned} \tag{4.6}$$

This gives us the simple result that the surface losses get more dominant the thinner the wires are, which is in line with previous studies on the subject [41, 51–53], which includes not just torsional modes (of which there isn't much data), but also that of flexural modes This also points to the way forward: tackling surface losses would be the key to achieving high Q for fibres, once clamp losses have been taken care of.

While eq.4.6 is not applicable to other modes of resonance, the direct inverse proportionality with the characteristic length of the samples still hold, which can be easily seen by dimension analysis.

In terms of values measured, [37] is the current record holder. Fused silica fibres have been shown to have higher Q than competing materials at room temperature, and my personal analysis of the situation is that these high Q fibres are drawn with a flame, resulting in an impeccable flame polished surface. This is not done with sapphire and silicon in existing literature (to my knowledge), possibly due to the higher melting temperatures. In addition, annealing was always applied, which helps to improve the bulk Q.

Cryogenic temps result in higher Q in general, with Al5056 [34] being a popular choice for metals. This has lead to the usage of Al5056 in cryogenic Weber bars, with high Q being a necessity for detection. As an aside, high Q is required for Weber bars precisely because the transfer function peaks higher at resonance, which is the opposite reasoning from lowering thermal noise with high Q.

4.4 Thermoelastic Damping

Sapphire is often not considered a suitable material for high Q fibres at room temperatures, with measured values for flexural modes generally being lower than silica by at least an order of magnitude [30, 49]. This is generally attributed to the thermoelastic effect. The

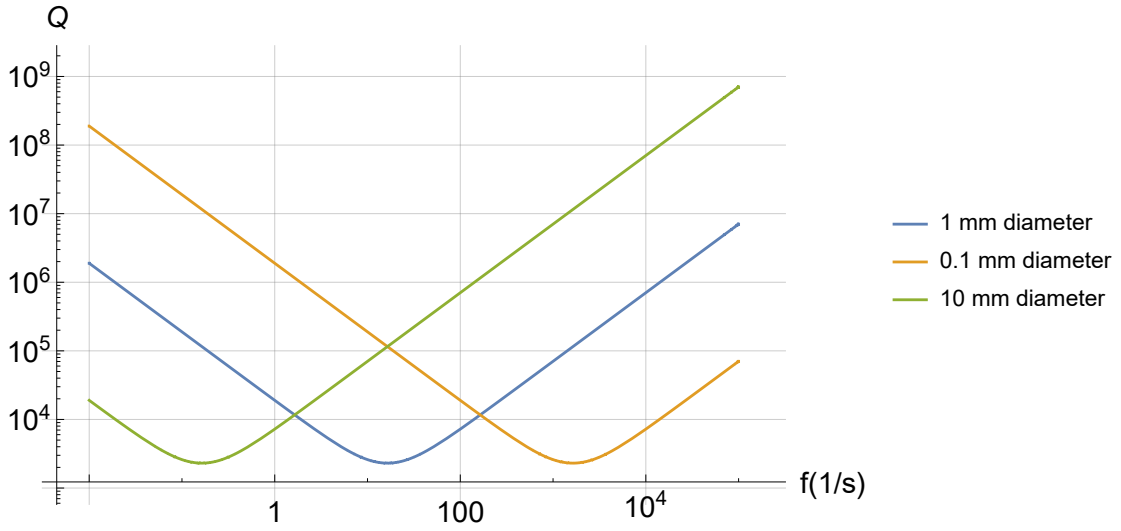

FIGURE 4.1: loglog plot of thermoelastic Q for various diameters of sapphire fibres, undergoing flexural motion. The values $Y = 350\,\mathrm{GPa}$, $\alpha = 5 \times 10^{-6}\,\mathrm{K}^{-1}$, and $\lambda = 23\,\mathrm{W\,m^{-1}\,K^{-1}}$ were used. Note that while different diameters shift the curve in the graph, it does not change the minimum Q of $\simeq 2 \times 10^3$. This graph is consistent with the Q measured for sapphire wires at room temperatures, as seen in [30, 49].

damping from this effect has been shown to provide a upper limit on the Q of the fibres over a variety of materials [49]. As we will later see, this limit does not apply to the torsion modes. Nonetheless, Q from thermoelastic damping will be derived here, for analysis purposes.

For thermoelastic damping in flexural modes [55, 56], the loss angle for structure damping is given by

$$\phi(\omega) = \frac{\Delta_r \omega \tau_r}{1 + (\omega \tau_r)^2}, \tag{4.7}$$

where Δ_r is known as the relaxation strength and τ_r is known as the relaxation time and is given by

$$\Delta_r = \frac{Y \alpha^2 T}{c} \tag{4.8}$$

and

$$\tau_r = \frac{c D^2}{2.16\,(2\pi)\,\lambda} \tag{4.9}$$

for circular rods, with α being the coefficient of thermal expansion, c the volumetric heat capacity and λ the thermal conductivity.

Inputting the values, for sapphire and considering a 1 mm thick fibre, the Q from the thermoelastic effect peaks at $\omega = \tau_r^{-1}$, and is right in the TOBA band, as shown in figure 4.1.

[49] suggests that at least for tungsten, the thermoelastic effect provides a celling for Q, but the loss angle is approximately independent of frequency, suggesting that the thermoelastic effect cannot simply explain internal friction. On the other hand, [30] suggests that for most metals, the loss angle can be modelled by

$$\phi(\omega) = \phi_0 + \frac{\Delta_r \omega \tau_r}{1 + (\omega \tau_r)^2}, \tag{4.10}$$

i.e. a frequency independent term added to the thermoelastic damping, but with fitted values of Δ_r and τ_r significantly deviating from theory.

Note that while thermoelastic damping's frequency dependence changes with thickness, it does not change the minimum thermoelastic Q. It therefore cannot explain the surface to volume ratio dependence of Q that the surface loss hypothesis can.

4.5 Experimental Concerns

In doing a ringdown experiment to measure Q, there are many possible loss mechanisms that can interfere with the energy dissipation, thus obscuring the true value of the internal friction of the samples being tested.

4.5.1 Gas Damping

Gas damping is the reason why the experiments are done in vacuum. As stated in the earlier sections, there are multiple mechanisms for energy dissipation, and they all affect the measured Q.

The Q from gas damping at low pressures is given by [57] as

$$Q_{gas} = \pi f_0 \frac{m}{4S} \frac{1}{n\sqrt{m_{molecule} k_B T}}, \tag{4.11}$$

where S is the surface area of the oscillator, n the number density of of the gas molecules, and $m_{molecule}$ the mass of the individual gas molecule. Presumably, S is the effective surface area in which the system is moving against the gas. This is taken into account in [29], where the relevant equation is modified to

$$Q_{gas} = 2\pi f_0 C \rho l \frac{1}{n\sqrt{m_{molecule} k_B T}}, \tag{4.12}$$

where C is a dimensionless constant that defers by shape, ρ is the density of the oscillator, and l is the characteristic length of the oscillator. This equation essentially replaces $\frac{m}{4S}$ with $2Ch\rho$, and thus are more or less equivalent to an order of magnitude.

4.5.2 Clamp Loss

Once gas damping is taken care of via putting the system in vacuum, the biggest limiting factor is that of clamp loss. This is generally the reason why the measured Q is lower than what is expected, across a wide variety of experiments. The equivalent to this for bulk measurements is that of the suspension system used to hold the resonator, where a simple change can affect Q drastically, for example, see [8], where a switch from silk to tungsten suspension fibres almost doubles Q. Unfortunately, there is no real way to calculate the extent of clamp losses, and can only be inferred.

4.5.3 Recoil Damping

Some energy in the system will also be transferred to the support via recoil. This is a area in which measurements of bulk Q via resonators have an advantage, as they can be supported at their nodal points, eliminating recoil to a great extent [5–7, 11, 35]

The effective Q from considering recoil damping is given by[29]

$$\frac{1}{Q_{effective}} = \frac{1}{Q} + \frac{1}{Q_{support}} \frac{m}{m_{support}} \frac{\omega_{support}{\omega_0}^3}{\left({\omega_{support}}^2 - {\omega_0}^2\right)^2}, \tag{4.13}$$

with $\omega_{support}$ being the resonance frequency of the support. This equation comes about from modeling the support structure as another oscillator coupled with the first. This means that when the support structure has a resonance frequency close to that of the system, the effective Q becomes much lower. In the case where $\omega_{support} \gg \omega_0$, as in the case of a larger rigid structure, the Q limit from recoil damping becomes

$$Q_{recoil} \simeq Q_{support} \frac{m_{support}}{m} \left(\frac{\omega_{support}}{\omega_0}\right)^3, \tag{4.14}$$

as seen in [58].

Interestingly, there appears to be a dissenting opinion, with Q_{recoil} given as [59, 60]

$$Q_{recoil} = Q_{support} \frac{k_{support}}{m{\omega_0}^2}, \tag{4.15}$$

where $k_{support}$ is the spring constant of the support. If we apply the relation $\omega^2 = \frac{k}{m}$, we end up with

$$Q_{recoil} = Q_{support}\frac{m_{support}}{m}\left(\frac{\omega_{support}}{\omega_0}\right)^2, \tag{4.16}$$

differing from the earlier model by a factor of $\frac{\omega_{support}}{\omega_0}$. Unfortunately, there is no explanation of this equation, so we cannot evaluate the reasoning behind this difference[1].

Converting the equations for use with torsion, we simply replace the mass ratio with that of the ratio of the moment of inertia, giving

$$Q_{recoil} \simeq Q_{support}\frac{I_{support}}{I}\left(\frac{\omega_{support}}{\omega_0}\right)^n, \tag{4.17}$$

where n is either 2 or 3.

A point to note about recoil losses is that the actual thermal noise profile away from resonance will be very different than what would be expected from a direct application of the measured Q at resonance to the equations found earlier in this chapter [29].

4.5.4 Coupling with Pendulum Mode

Due to the imperfection of the system used, there will be some coupling with the pendulum mode. This will lead to energy being transferred, and lost via this mode. A model for this is currently being developed.

4.5.5 Amplitude Dependence of Q in Torsion Pendulums

An amplitude dependence of Q has been observed for torsion pendulums, for a variety of materials [3, 23, 28] at both room and cryogenic temperatures. In particular, [23] shows that while metals have a linear relation between Q^{-1} and amplitude, sapphire does not. While this will not affect TOBA as it is operated only at small amplitudes, this will affect the measured Q in ringdown measurements. [23] suggests that at 4.2 K, a peak shear strain of less than $\gamma_0 < 1 \times 10^{-4}$, Q drops by less than half.

4.5.6 Q Corrections from Noise Floor

In any real experiment, noise enters from seismic motion of the ground. To understand the effect this has on the data, we shall construct two simplified models to quantify this effect.

[1] Further muddying the waters we have a case of $\frac{{\omega_{support}}^2{\omega_0}^2}{\left({\omega_{support}}^2-{\omega_0}^2\right)^2}$ in [61], but simply cites [29].

4.5.6.1 Energy Based Noise Floor

The first uses an energy argument. We assume that the energy enters the system at a constant rate, given by ΔE_s per cycle. This means that the measured Q is related to this term by

$$Q_{measured} = 2\pi \frac{E}{\Delta E} = 2\pi \frac{E}{\Delta E_d - \Delta E_s}, \tag{4.18}$$

where ΔE_d is the energy dissipated by the setup. Note that this is not the net energy dissipated, which is given by $\Delta E_d - \Delta E_s$.

This can be rewritten as

$$\frac{1}{Q_{measured}} = \frac{1}{Q_{setup}} - \frac{1}{2\pi}\frac{\Delta E_s}{E}. \tag{4.19}$$

We now consider the case in which the system has reached the noise floor. In this case, $\Delta E_d = \Delta E_s$. We shall call the system energy in this steady state E_{ss}. We can now rewrite the above equation to

$$\begin{aligned} \frac{1}{Q_{measured}} &= \frac{1}{Q_{setup}} - \frac{1}{2\pi}\frac{\Delta E_s}{E_{ss}}\frac{E_{ss}}{E} \\ &= \frac{1}{Q_{setup}} - \frac{1}{Q_{setup}}\frac{E_{ss}}{E} \\ &= \frac{1}{Q_{setup}}\left(1 - \frac{E_{ss}}{E}\right). \end{aligned} \tag{4.20}$$

Finally, we note that energy is proportional to the square of the amplitude (of any simple harmonic motion system), so

$$Q_{measured} = \frac{Q_{setup}}{1 - \frac{{a_{ss}}^2}{a^2}}, \tag{4.21}$$

where a is the amplitude and a_{ss} is the amplitude at steady state. This equation allows us to evaluate qualitatively at which point above the noise floor the measurements can be trusted. Note that the measured Q shows up as proportional to the gradient in a semi log plot of amplitude to time, so strictly speaking, $Q_{measured}$ in the above argument only applies to the gradient at a specific point, and not the best fit line that would be used to measure Q, as that will depend on the initial amplitude.

Putting our model in action, if we take a 10% change in the term $1 - \frac{{a_{ss}}^2}{a^2}$ as the limit, we have

$$\frac{a_{ss}}{a} = \sqrt{0.1} \simeq 0.316, \tag{4.22}$$

meaning that as long as we take data above 3 times the noise floor, the noise floor isn't an issue.

4.5.6.2 Amplitude Based Noise Floor

The second model simply models the noise floor as an additional constant to the ringdown amplitude. This is an argument from a force based noise, as force is proportional to amplitude. The amplitude is now

$$a = e^{\frac{\pi f_0}{Q}t} + a_{ss}, \tag{4.23}$$

as compared to the case without noise of $a = e^{\frac{\pi f_0}{Q}t}$.

4.5.6.3 Comparisons of the Two Models

In order to do a comparison of the two models, we need to rewrite the energy based noise floor model into a amplitude equation like we have for the amplitude based noise floor. We start out with

$$a = e^{\frac{\pi f_0}{Q_{measured}}t} = e^{\frac{\pi f_0}{Q}\left(1-\frac{{a_{ss}}^2}{a^2}\right)t}, \tag{4.24}$$

where Q is Q_{setup}. This is then solved, giving

$$a = \sqrt{\frac{{a_{ss}}^2 2\pi f_0 t}{W\left(\frac{2{a_{ss}}^2\pi f_0 t}{Q}e^{\frac{\pi f_0}{Q}t}\right)Q}}, \tag{4.25}$$

where $W()$ is the Lambert W function.

We now can evaluate the two approaches on an equal footing. Figure 4.2 shows how the two models compare with each other.

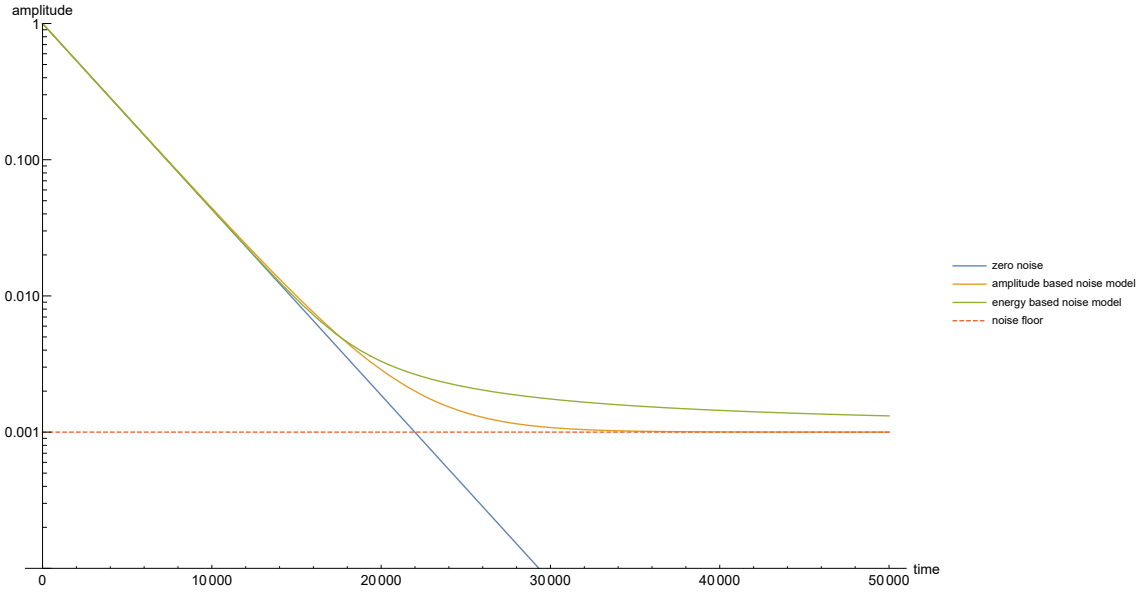

FIGURE 4.2: Logplot of the amplitude with time for the two noise model, coupled with the no noise ideal line and the noise floor (dashed). Note that the amplitude model reaches the noise floor much faster, but the overall look of both models are similar, and are probably fairly approximates the noise situation to a similar accuracy empirically. Considering that Both models suffer from not modelling the noise realistically, especially sudden spikes, which would actually affect the data above the noise floor.

Chapter 5

Experimental Setup

5.1 Experimental Overview

The torsional Q factor for fibres were measured via the ringdown method, which was explained in detail in the previous chapter. Simply put, a system is allowed to resonate and then left alone, with the resonance frequency and decay in amplitude measured. A more direct measurement would be to measure the thermal noise directly in the off resonance region, but that is unfeasible because of the sensitivity required.

For our experiments, 1 mm fibres were used. 15 mm sapphire fibres were procured from Orbe Pioneer and Impex, while 10 m of Copper Beryllium fibre was obtained from Nilaco. Both a C-axis and a A-axis fibre from Orbe Pioneer were measured, while only a C-axis fibre from Impex was measured. Sapphire was chosen because of its low internal friction, and its excellent performance at cryogenic temperatures [10].

5.2 Experimental Setup

The first experimental setup was a generic torsion pendulum setup. A disc was chosen instead of a bar so as to reduce the asymmetry of the system, reducing possible loss via the setup.

Care was taken to handle the fibres as delicately as possible, both to prevent breakage as well as unnecessary surface damage, which has been seen to lower Q [50]. Nonetheless, some damage was unavoidable, and this could have lead to lower Q then what the original samples had.

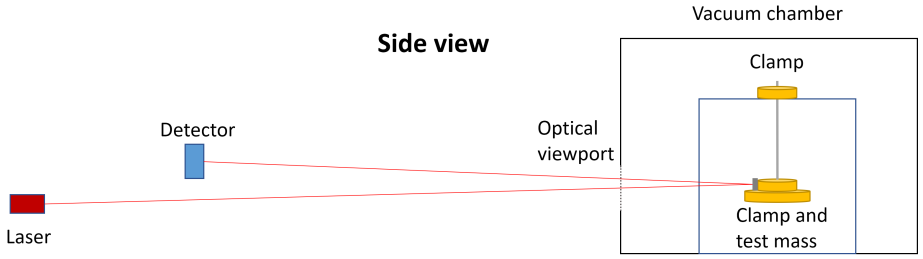

FIGURE 5.1: Schemetic of the setup, side view

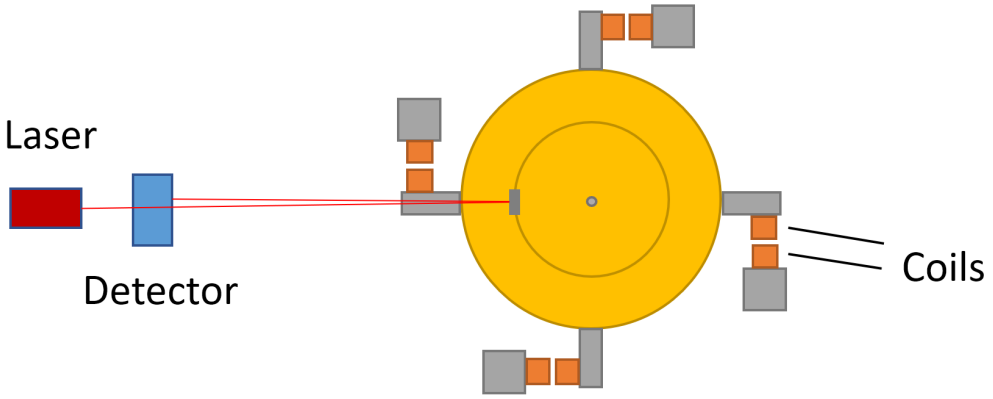

FIGURE 5.2: Schemetic of the setup, top view

5.2.1 Clamps

The clamps (for the 1 mm fibres) were designed with a 1 mm radius hole, but with a gap of 0.2 mm. This ensured adequate leeway for clamping, while maintaining good contact with the fibre. This design was conceived as a way to deal with crystalline wires that do not deform, which implies that standard flat clamps would provide poor contact and thus poor clamping strength when used with crystalline wires. In addition, using flat clamps would most likely lead to deformation of the metallic clamps, leading to lower clamping strength with time [48].

Contrast this with clamping thin metal fibres with flat clamps; the fibre deforms and this deformation drastically reduces slipping. Naturally, a larger clamp strength and lower contact area would lead to greater deformation, reducing friction losses from the clamp, as seen in [62]. This is but one of the challenges faced in dealing with crystal fibres.

The clamps were clamped onto the stage via m4 screws.

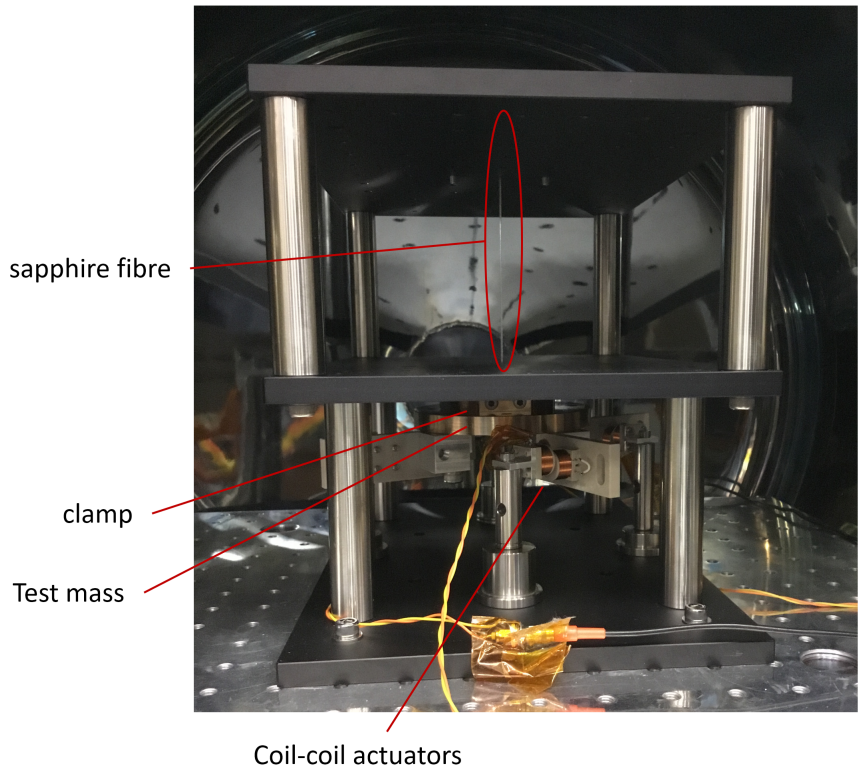

FIGURE 5.3: Picture of the experimental setup, with a C-axis sapphire fibre from Orbe Pioneer.

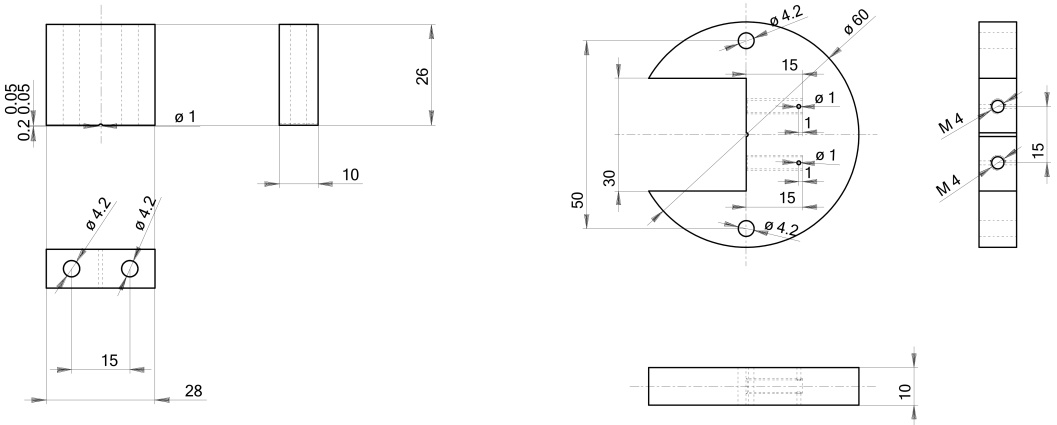

(A) (B)

FIGURE 5.4: Schematics for the different parts of the clamps. Note the hole in the centre to accommodate the sapphire fibre. The clamp is designed to have a 0.2 mm gap when clamped, to allow for variance of the fibre diameter, as well as manufacturing inaccuracy.

TABLE 5.1: various setup dimensions

Setup Dimensions	
Diameter of fibre (sapphire, CuBe)	1 mm
Length of fibre (sapphire)	15 cm
Length of fibre (CuBe)	~15 cm
Effective length of fibre between clamps	~12.5 cm
Mass of a clamp	219 g
Mass of one coil attachment	48 g
Mass of the test mass	~650 g
Moment of inertia of clamp with two coils	$\sim 2.6 \times 10^{-4}$ kgm^2
Moment of inertia of test mass with clamp and with four coils	$\sim 1.6 \times 10^{-3}$ kgm^2
Clamp thickness	1 cm
Clamp diameter	6 cm
test mass thickness	1 cm
Test mass diameter	10 cm

5.2.2 Test Mass

The test mass was made from copper beryllium, with a diameter of 10 cm and thickness of 1 cm, and is attached to the clamp via 2 m4 screws. It also has 8 holes equidistant from the edge for mounting purposes. These holes were used to mount the coils used for driving torsion resonance.

5.2.3 Stage

The stage was built by combining two adjustable adapter kits UP-2030 from Sigma Koki, with 100 mm tall posts. These kits are made up of two anodized aluminium plates, 300 mm long, 200 mm wide, and 10 mm thick with four stainless steel posts. The stage was designed with 2 levels to test a design we would like to call dual clamp mode.

5.2.4 Dual Clamp Mode

Dual clamp mode was designed for a few reasons; firstly, it good at suppressing the pendulum mode, as it is held on both ends. Secondly, it allows for a larger effective angular spring constant of

$$\kappa_{effective} = \kappa_u + \kappa_l, \tag{5.1}$$

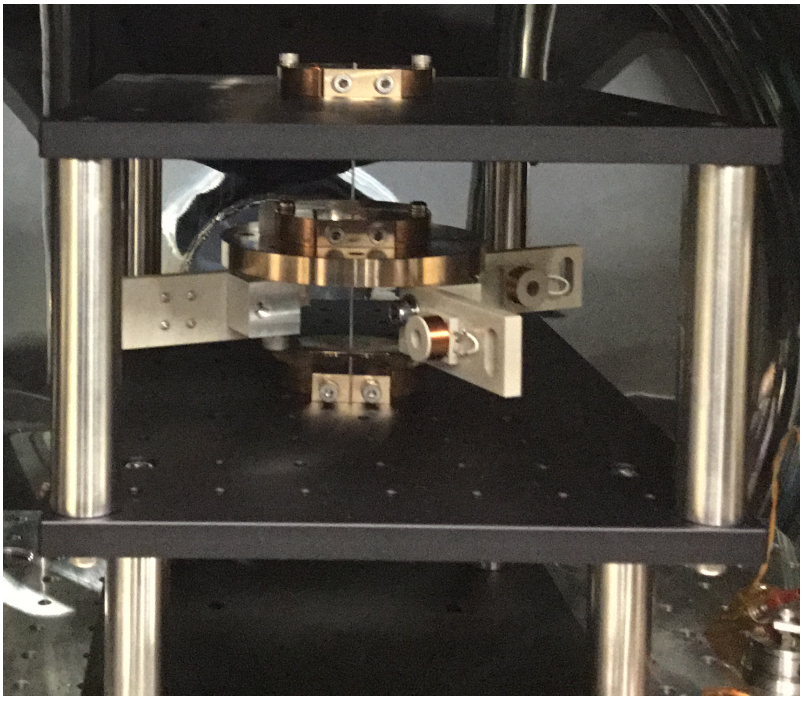

FIGURE 5.5: Picture of the experimental setup in dual clamp mode. The top clamp is also visible here. In this picture, the pairing sets of coils have not yet been added. The mirror on the left side of the clamp is clearly visible.

where κ_u and κ_l represent the angular spring constant of the upper and lower sections of the fibre respectively. These two effects mean that the noise floor in this mode is much suppressed.

This larger angular spring constant, coupled with the shorter fibre provided, allows us to study higher angular frequencies, which can help with studying the frequency dependence, or lack thereof of the measured Q. This mode will be studied further, as it will be expected to help provide further insights into unwanted loss mechanisms, and provide different frequency data.

5.2.5 Low Mass Mode

Low mass mode is a configuration that does away with the test mass, and let's the clamp itself be the torsion pendulum. Being lighter, it reduces the clamp losses.

5.2.6 Coil-Coil Actuators

Coil-coil actuators were used to excite the setup for the ringdown measurement to take place. The wires were physically disconnected after excitation to prevent noise from the wires from effecting the ringdown by providing additional energy. The output was set at

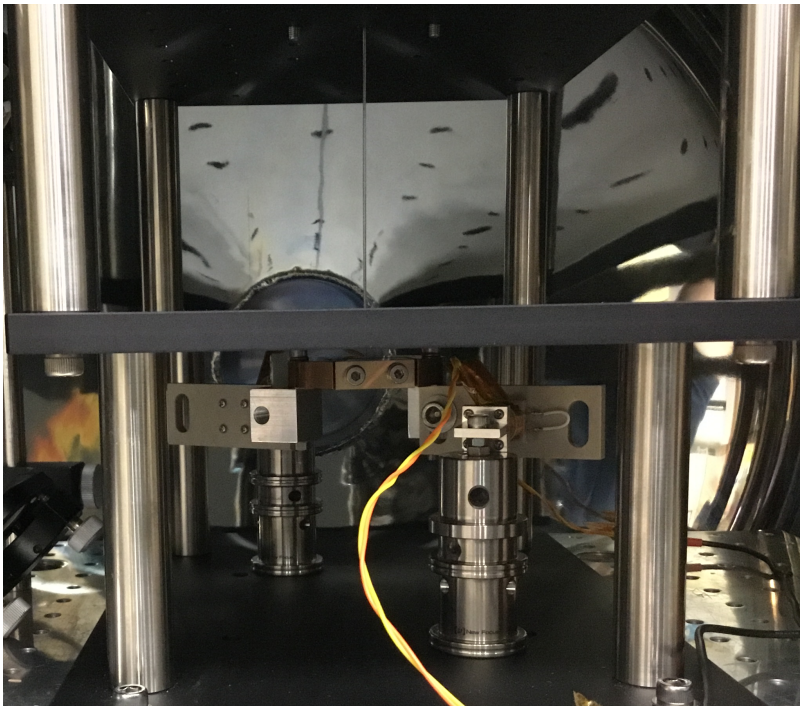

FIGURE 5.6: Picture of the experimental setup in low mass mode. In this mode, the clamp itself is the torsion pendulum, and only two sets of coils are used.

1500 Hz, at 2 V, which was connected to a circuit that converted it to a .2 A output. It was found to provide a force of about 2×10^{-4} N for each set of coils, which was enough to excite the system if pulsed at a the resonance frequency. Four sets were used in the normal mode, while two sets were used in the low mass mode. They can be seen clearly in fig 5.3.

5.2.7 Optical Lever

The setup uses a optical lever for the data readout, and data is recorded via Moku:Lab by Liquid Instruments. The sensor used was a laser positional sensor, and was positioned approximately 1 m away from the crystal fibre. The sensor hole has a size of 1.3 cm, allowing for the measurement of around 1 cm worth of movement, corresponding to about 10 microrad, and thus an angular amplitude of 5 microrad.

5.2.8 Clamp Strength

A hex key was used on the m4 screws to fix the fibres to the clamps. The screw torque was varied via choosing the length of the lever arm of the hex. A torque wrench was not used due to the geometry of the setup, leading to clearance issues preventing it from being

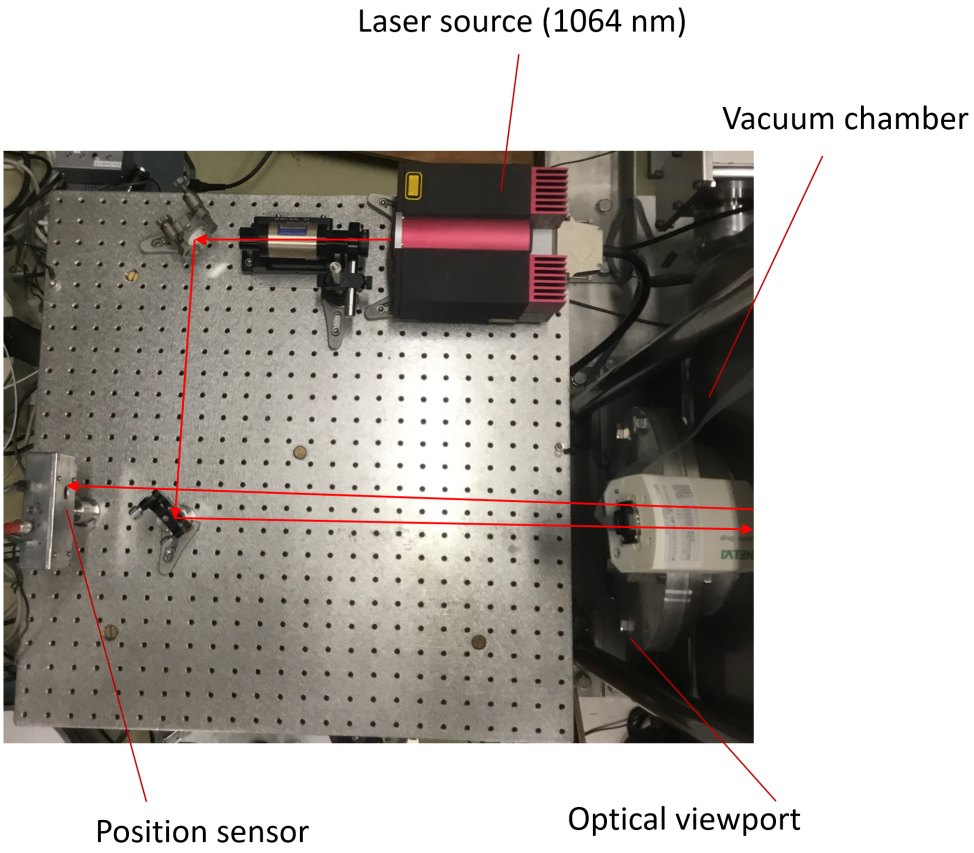

FIGURE 5.7: Picture of the optical table used. The position of the mirror and the position sensor is not fixed, and is adjusted every time the configuration changes, because there is no way to adjust the position of the test mass once clamped.

used. However, comparison outside the setup quantifies high strength to be $\sim 1.5\,\mathrm{N\,m}$, with low strength being $\sim 0.5\,\mathrm{N\,m}$

5.3 Experimental Details

A Copper Beryllium fibre was first used in the the standard setup, at high clamp strength, for setup testing. $Q = 1.4 \times 10^4$ was measured, and tallied with cantilever measurements of Q seen in [30]. Unfortunately, the rest of the experiments did not go as smoothly.

An Orbe Pioneer C-axis sapphire fibre was used in the the standard setup, at high clamp strength. This fibre was unpolished, and had its diameter measured with a micrometre screw gauge at 4 points, ranging from 1.008 mm to 1.030 mm. This resulted in the largest measured Q of $Q = 1.3 \times 10^5$. Unfortunately, this also resulted in the fibre snapping at the clamp points, which means that this is rather too destructive for budgetary reasons. While this was still unbeknownst, the dual clamp setup was tested, and

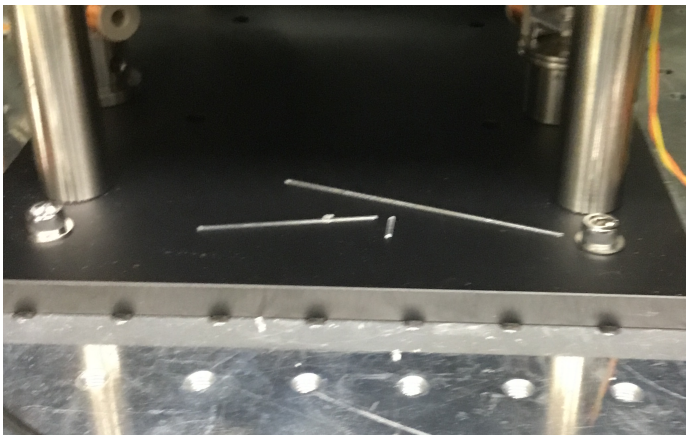

FIGURE 5.8: Picture of pieces of the Orbe Pioneer C-axis sapphire fibre.

the Q was found to be $Q \sim 4 \times 10^4$. The reason why the fibre snapping was not known at this point was due to the top clamp remaining clamped and the broken piece from the test mass clamp was so tiny as to be not noticeable without looking for it. It is believed that the low Q for this set of measurements were due to improper handling.

This led to testing with the low clamp strength mode, and led to $Q \sim 2 \times 10^4$, but it was found that the longest remaining fibre fragment at about 9 cm long used did not snap. This was then tested with an Orbe Pioneer A-axis sapphire fibre, at both a standard pendulum mode at approximately 5 cm fibre length and dual clamp mode, to produce $Q \sim 2 \times 10^4$ for both. This fibre was similarly unpolished, with a similar diameter.

At this stage, the clamp loss was the biggest suspect in terms of Q limiting losses, and it was decided that lowering the load might help with it. It was then set to low clamp strength low mass dual clamp mode, but the resonance frequency became too high to excite via the current system, and thus was then reset to a standard mode (but at low mass), where $Q = 9 \times 10^4$ was measured. This suggested that the clamp losses were reduced by a lower load, reducing stick/slip losses. This setup was then repeated with a polished C-axis fibre from Impex, which resulted in $Q \sim 2 \times 10^4$. The clamps were then tighten to high strength mode, increasing Q to 7×10^4, but this resulted in the fibre snapping.

Chapter 6

Results and Discussion

All data analysis was done via Mathematica 10.4. An exponential curve was fitted to the amplitude of the ringdown, which coupled with the resonance frequency as measured by the Fourier transform, gives us the measured Q via $Q = \pi f_0 \tau$. Figure 6.1 shows a typical ringdown curve for each of the values tabulated in table 6.1.

From the ringdown curves, we can see that it is well modelled by an exponential decay, especially if we ignore the noise floor and some noise spikes.

The copper beryllium measured Q was in line with previous measurements of CuBe wire [30], suggesting that the setup was working as designed. However, the CuBe wire

TABLE 6.1: Table of torsion Q values. At least three ringdowns were collected for each entry in the table. The uncertainties were estimated from the spread of values of the various ringdowns, with all measured values fitting into the error bars. The values in red are the highest values for each sample. Ironically, the sample that is polished ended up with a lower Q than the unpolished ones. This is likely due to a lower coefficient of friction between the clamps and the fibre, leading to greater clamp losses.

	High clamp strength	**Low clamp strength**	**Low clamp strength at low mass**	**High clamp strength at low mass**
Niraco Copper Beryllium	$(1.4 \pm 0.2) \times 10^4$			
Orbe pioneer sapphire c-axis (unpolished)	$(1.3 \pm 0.3) \times 10^5$	$(2.4 \pm 0.8) \times 10^4$		
Orbe pioneer sapphire a-axis (unpolished)		$(1.8 \pm 0.3) \times 10^4$	$(8.8 \pm 0.8) \times 10^4$	
Impex sapphire c-axis (polished)			$(2.5 \pm 0.3) \times 10^4$	$(6.7 \pm 0.9) \times 10^4$

Low mass ~300 g, standard setup ~1 kg

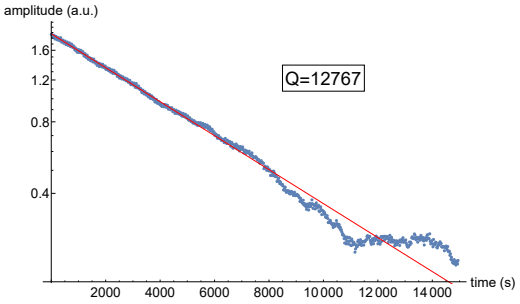

(A) Logplot of a ringdown for the CuBe fibre, with fitted Q

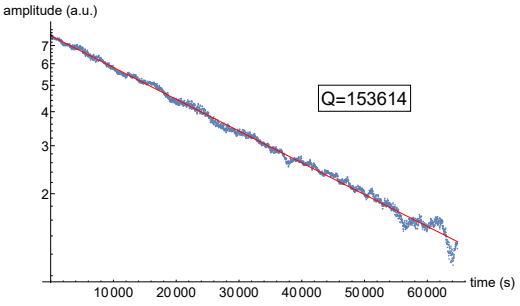

(B) Logplot of a ringdown for the Orbe Pioneer sapphire c-axis fibre at high clamp strength, with fitted Q

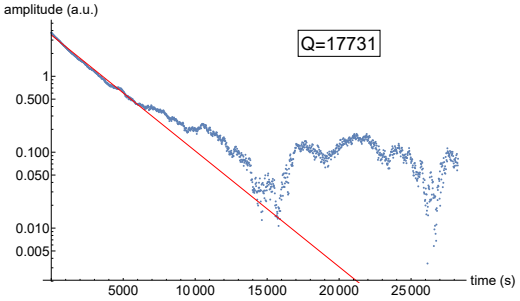

(C) Logplot of a ringdown for the Orbe Pioneer sapphire c-axis fibre at low clamp strength, with fitted Q

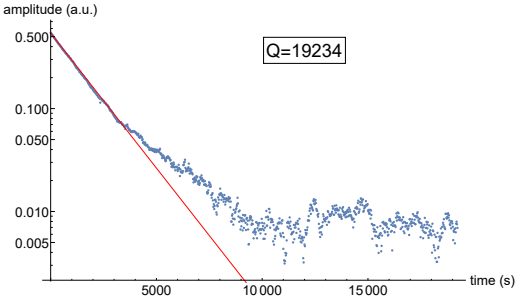

(D) Logplot of a ringdown for the Orbe Pioneer sapphire a-axis fibre at low clamp strength, with fitted Q

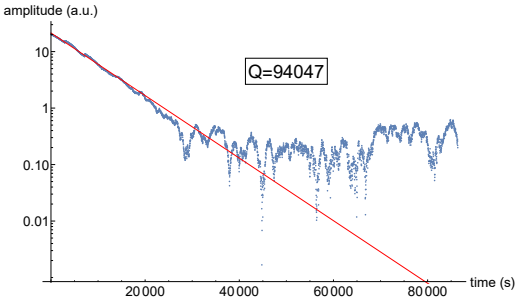

(E) Logplot of a ringdown for the Orbe Pioneer sapphire a-axis fibre at low clamp strength at low mass, with fitted Q

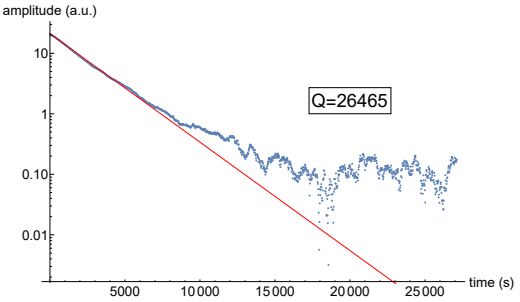

(F) Logplot of a ringdown for the Impex sapphire c-axis fibre at low clamp strength at low mass, with fitted Q

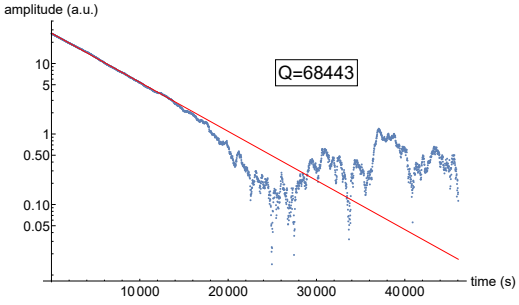

(G) Logplot of a ringdown for the Impex sapphire c-axis fibre at high clamp strength at low mass, with fitted Q

FIGURE 6.1: Sample logplots all the data in table 6.1. Notice how the background noise fluctuate greatly, but is not allowed the ringdown fit noticeably by only considering the high amplitude region.

had a quirk that the sapphire fibres did not; it was slightly curved. Weights were added to correct for this curve, in order to have the torsion pendulum approximately parallel to the ground. This could have lead to greater coupling between pendulum modes and the torsion mode, due to further symmetry breaking.

A c-axis sapphire fibre from Orbe Pioneer was measured with the torsion pendulum setup to have $Q = 1.3 \times 10^5$ at 1.31 Hz. This is the highest Q measurement for a sapphire fibre at room temperature (as far as this author knows), with only cryogenic measurements being up to two orders of magnitude higher [48] and room temperature measurements being one order of magnitude smaller [30, 49]. On the other hand, a bulk measurement of sapphire at room temperature shows values up to $Q = 6.4 \times 10^7$[7] and 2.7×10^8[8], which suggests that we are far from unlocking the true potential of sapphire. Refer to Table 4.3 for other sapphire Q measurements.

The significance of this achievement can be seen by comparing it with initial LIGO's use of steel music wires, with an estimated $Q = 3 \times 10^3$ [63, 64]. Having surpassed this result by two orders of magnitude without any treatment of of the sapphire showcases the potential of crystal fibres.

While it is unfortunate that the clamp strength required for this caused the fibre to snap, it must be noted that the suspension did not fail, and is perfectly viable as an experimental system.

This result can be interpreted as surface loss dominant, and suggests that sapphire is usable for TOBA, as long as the surface loss is reduced to the extent that Q increases by three orders of magnitude via cryogenic cooling and other techniques.

In cantilever modes, the existing literature shows an increase of 5×10^3 to 10^7 via cryogenic cooling, but due to different methodologies, it cannot be stated for certain how accurate the measured values are compared with the actual sample quality. In general, experiments tend to understate Q, due to various dissipative mechanisms that increase the energy loss, leading to a lower measured Q than that of the actual Q by the internal friction of the sample.

The other samples achieved lower values, mainly due to lower clamped strength used to prevent breakage of the sapphire fibres.

TABLE 6.2: Table of measured frequencies. Note that there is two frequencies for the pendulum mode due to the imperfection of the stiff sapphire fibres. There is no pendulum mode in the dual clamp mode.

material	Torsion frequency (Hz)	Pendulum frequency (Hz)
CuBe	0.667	1.38, 1.39
Orbe Pioneer C-axis sapphire	1.313	1.53, 1.54
Orbe Pioneer C-axis sapphire, low strength, shorter fibre	1.985	2.51, 2.53
Orbe Pioneer A-axis sapphire low strength, dual clamp mode	3.699	
Orbe Pioneer A-axis sapphire low mass, low strength	3.818	1.911, 1.98
Impex C-axis sapphire low mass, low strength	3.477	2.01, 2.07
Impex C-axis sapphire low mass, high strength	3.493	2.01, 2.07

6.1 Measured Frequency

The frequencies are measured via the peaks in the Fourier transforms, and are tabulated in table 6.2. Fig 6.2 shows how the ringdown looks like in frequency space. The measured values differ from the ones calculated in eqn 2.11 within 10%, using the values $\mu = 150\,\text{GPa}$, $\rho_{CuBe} = 8200\,\text{kgm}^{-3}$. This discrepancy can be attributed to the simplifications in the modelling of the moment of inertia of the system, along with uncertainty over the precise shear modulus to be used. In any case, this level of discrepancy is in line with other works that utilise torsion resonance ([5], among others).

6.2 Surface Loss

Surface loss, which is widely believed to be the dominant limiting factor for the internal friction of fibres, could not be measured properly, due to clamp losses. However, we can do an estimate of the expected loss by looking at [7], where a torsion mode was measured with a $Q = 9.2 \times 10^6$ for cylinder sample with length of 6 cm and diameter of 10 cm. Using the values of $\frac{1}{Q_{surface}} h = 1.3 \times 10^{-9}\,\text{m}$ and $Q_{bulk} = 3.4 \times 10^7$ from [7], we then apply it to

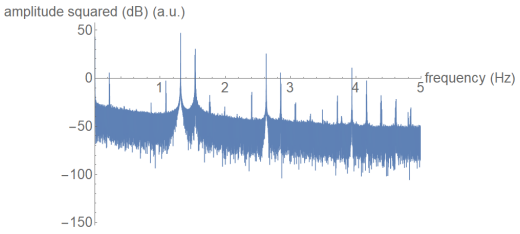

(A) Frequency spectrum of a ringdown. This graph is plotted on a decibel scale, to better identify peaks.

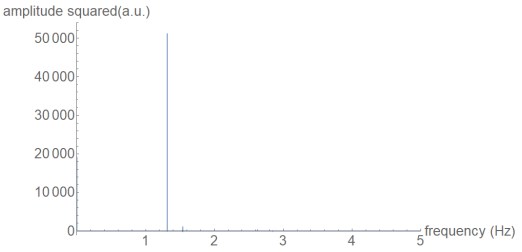

(B) Same frequency spectrum of a ringdown, with an absolute scale. Note how difficult it is to distinguish other peaks like this.

FIGURE 6.2: Frequency spectrum of a C-axis sapphire fibre ringdown. The peak at 0 Hz correspond to the offset between the neutral position of the system and the zero of the optical sensor. The peak at 1.31 Hz correspond to the torsion resonance frequency, and the peak at 1.5 Hz correspond to the pendulum mode. Multiples of these resonances correspond to the deviation from perfect sinusoidal curves.

eqn 4.5, for a 1 mm thick fibre, we obtain

$$\begin{aligned}\frac{1}{Q_{eff}} &\sim \frac{1}{Q_{bulk}} + \frac{1}{Q_{surface}} h \frac{\int_S \gamma^2 dS}{\int_V \gamma^2 dV} \\ &= \frac{1}{3.4 \times 10^7} + 1.3 \times 10^{-9} \frac{8}{1 \times 10^{-3}} \\ &= \frac{1}{9.6 \times 10^4}.\end{aligned} \tag{6.1}$$

This meant that the best results obtained here are in line with the results obtained by [7], and shows that our result are probably not limited by other loss mechanisms, for the unpolished fibres. This data also lends credence to the notion that $Q_{surface}$ is frequency independent, as the resonant frequencies measured here are in the order of $\sim 1\,\text{Hz}$, where the values in [7] are around $\sim 50\,\text{kHz}$. We note that just like in [7], we have, at the curved surface, small scratches and pits visible to the naked eye. This suggests a similar amount of surface damage, and thus justifies the similar values of $\frac{1}{Q_{surface}} h$. This result is graphed in fig 6.3.

Unfortunately, clamp loss seems to be larger for the polished fibre, which can be attributed to a lower coefficient of friction due to surface smoothness.

6.3 Pendulum Mode

For comparison purposes, the Q of the pendulum mode was also measured. This is so that comparisons between the flexural mode, where thermoelastic loss is a factor, can be compared with the torsion mode. The pendulum mode is related to the flexural fibre Q via something known as the dilution factor. The pendulum mode was cannot be activated by

FIGURE 6.3: The results from [7], extrapolated to this study's result. The purple line comes from setting the bulk Q as infinity, which clearly shows how dominated by surface loss 1 mm sapphire fibres are. This result suggests that the results currently obtained is limited mainly by surface loss, and not other damping mechanisms.

the coils, and thus is activated either by delivering an impulse on the vacuum chamber, or if an earthquake happens to occur during measurement. Due to the stiffness of sapphire, the low mass setup could not be reasonably excited to a reasonable extend above the noise floor using these methods.

6.3.1 Gravitation Dilution

In a pendulum, the measured pendulum Q is related to the fibre Q via the relation [29, 65]

$$Q_{pendulum} = Q_{fibre}\frac{2mgL}{\sqrt{F_T Y J}}, \tag{6.2}$$

where F_T is the tension of the setup, J the second moment of area of the fibre, and m is the mass of the pendulum. The factor next to Q_{fibre} is known as the dilution factor, and it comes from the fact that most energy is stored in the gravitational field while the energy is dissipated in the fibre for a pendulum. Note that there is no equivalent for a torsion pendulum, and the second moment of area here is $J = \frac{\pi D^4}{64}$, half of that of the polar moment of area used in torsion.

Unfortunately, for our setup, this equation is not valid, as it assumes a effective length (see fig 6.4) similar to the real length of the pendulum. The difference between the two

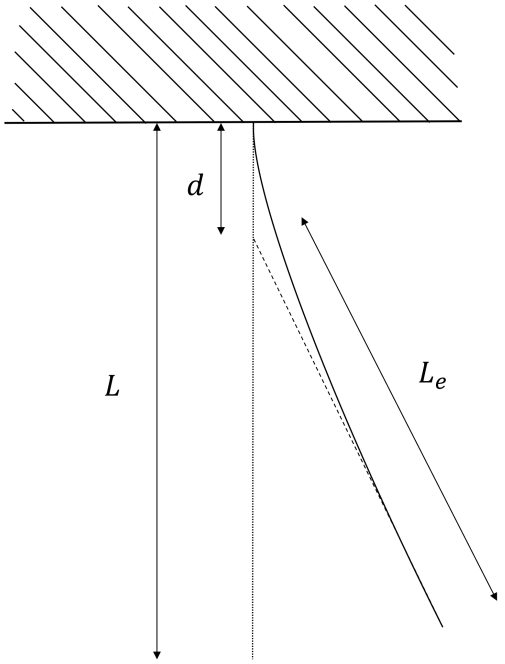

FIGURE 6.4: The relation between the effective length L_e and actual pendulum length L is shown here. The standard dilution factor, eqn 6.2, assumes $L_e \sim L$, which is not the case with the current setup.

lengths is given by

$$d = \sqrt{\frac{YJ}{F_T}}, \tag{6.3}$$

which for our setup is $\sim$ 4.2cm for normal and $\sim$ 7.6cm for the low mass mode. This means that the standard relation is obviously not applicable, so a form of the dilution factor without this assumption was then derived for use here. The details can be found in appendix A.

6.3.2 Pendulum Mode

For our C-axis Orbe Pioneer fibre, the pendulum Q was measured to be $\sim 4 \times 10^4$.

Applying the dilution factor of 4.1 for our setup to our measured values of $\sim 4 \times 10^4$ pendulum Q, we end up with $Q_{flexural} \sim 10^4$, which is consistent with being limited by themoelastic damping as seen in fig 4.1, and an order of magnitude smaller than the torsion mode. This is in line with other measurements [30, 49], where the measurements are also limited by themoelastic damping. This result is plotted in fig 6.5.

There are two peaks for the pendulum resonance, and they are very close. Considering how stiff sapphire is, and the thickness of fibre used in comparison to the weight, it is

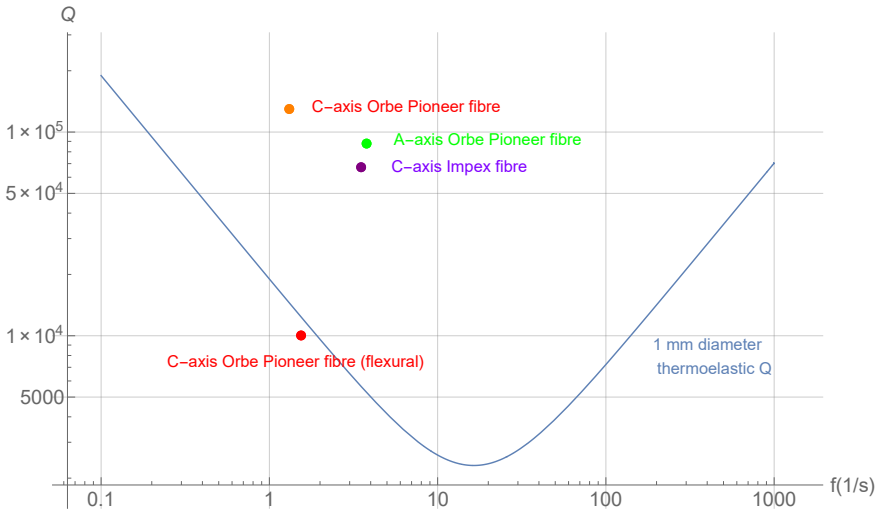

FIGURE 6.5: The best result for each sapphire sample is plotted here, along with the flexural value for the c-axis Orbe Pioneer fibre. The thermoelastic limit for flexural is also drawn here, where it can be clearly seen that the flexural Q obtained here is clearly limited by it, similar to [30, 49].

unsurprising that this behaviour also appears in the measurement of flexural modes, and is often attributed to deviations of the fibre from a perfect cylinder [48].

6.4 Clamp Loss

Clamp loss is probably the biggest loss source in these measurements, and that is due to the nature of clamps. While Coulomb losses being dominant can be ruled out due to the lack of a linear amplitude dependent damping [47], in practice clamp losses do not show up so simply, and is practically indistinguishable from internal damping [66]. This has lead to a widespread belief that many studies on high Q have been limited by clamp losses, as mentioned in [67]. For more details on possible clamp loss mechanisms, see [68]. To get around this issue, for the case of fused silica, making use of the method for drawing thin fibres via a flame from a thicker rod, the thicker section is often left connected to the fibre, with only the thicker section being clamped [49]. This essentially removes the need for clamping thin fibres.

While in our experiments we cannot eliminate the effects of the clamps completely, we can show the effects of clamp loss from the A-axis unpolished fibre and the C-axis polished fibre. The A-axis polished fibre had its Q increase when the torsion pendulum mass was decreased, suggesting that the lower weight reduced the amount of frictional losses. In the case with unpolished fibres, the lower Q obtained suggests that the smaller friction

coefficient probably have led to larger clamp loss, due to more slipping and thus energy loss occurring.

Unfortunately, increasing clamp strength in the current design lead to fibre snapping, both for the unpolished Orbe Pioneer C-axis fibre as well as the polished Impex C-axis one. The fragility of these fibres brings to mind the incident with Advanced Virgo, where the monolithic fused silica suspensions failed due to dust hitting the fibres [69], which reminds us of the difficulty in working with crystal fibres. The fragility of sapphire is also mentioned in [30].

6.4.1 Clamp Strength

Tests of clamp strengths were conducted with a snapped piece of the C-axis Orbe Pioneer clamped by an identical clamp to determine the breaking strength. It was found to snap when the torque applied on the m4 screws of the clamp were at 1.2 N m. This means that going forward, with this clamp design, the torque applied on these fibres should be limited to 1 N m. This study needs to be applied on the other fibre types, to see if the braking strength is similar.

6.5 Amplitude Dependence

While technically not a loss mechanism, as it is caused by the sample itself, amplitude dependence Q might affect wrongly affect the evaluation of samples, due to the effect only appearing in ringdown experiments and not in the actual thermal noise spectrum of an actual operational detector.

In this experiment, using the standard setup, we have peak shear strains of $\gamma_0 = r\frac{\theta_0}{L} = 2 \times 10^{-5}$, while for the dual clamp mode, that of $\gamma_0 = 5 \times 10^{-5}$, which are small enough to not not affect Q significantly, according to [23]. More importantly, the measured ringdowns exbibit linear behaviour in the logplots, which suggests that a significant change in Q did not happen as the amplitude decreases. Thus, this factor was considered insignificant compared to the measured uncertainty.

6.6 Additional Loss Mechanisms

As mentioned in section 4.5, any other energy losses will affect our measured Q. We will evaluate these concerns with respect to our experimental setup.

6.6.1 Gas Damping

Using the equation 4.11, and taking the conservative values of the pressure being 10^{-3} Pa, a frequency of 1 Hz, and assuming an all nitrogen atmosphere we see that we will easily get $Q_{gas} > 10^7$. As this is at least two orders of magnitude larger that all of our results, it will be ignored. Additionally, the measured Q does not increase from the first to the remaining runs of each sample, where the pressure generally drops by an order of magnitude across the testing of the sample, indicating that Q is not limited by the residual gas.

6.6.2 Recoil Damping

We estimate the properties of the support as $Q_{support} \sim 10^2$, $\frac{I_{support}}{I} \sim 10$ and $\frac{\omega_{support}}{\omega_0} \sim 10^2$, which gives us a $Q_{recoil} \gtrsim 10^7$ using equation 4.17 and can be ignored. In practice, it is often hard to estimate the recoil damping accurately, but the dependence on frequency means that it should change quite drastically with frequency, so if there is no dependence with frequency in the measured Q, it can be safely argued to be not recoil damping limited. In this experiment, a low mass setup with an Orbe Pioneer C-axis fibre at high clamp strength should be conducted, in order to rule it out conclusively.

6.6.3 Possible Loss Mechanisms

Further loss mechanisms that are not calculated include: possible electrostatic noise and coupling with pendulum mode. These possible losses should be modelled to ensure that they are not the limiting loss mechanisms. This will become more critical as Q increases.

6.7 Data Analysis Techniques

This section deals with the data analysis techniques used to extract the data from the raw signal. The most computationally expensive part of the data analysis was to extract out the amplitude. The most naive way would be to identify peak positions for each oscillation. However, this method would be incredibly computationally expensive, considering that the data collected has up to over 3×10^5 oscillations for each measurement. Furthermore, this method becomes inaccurate when noise becomes a significant percentage of the amplitude. Thus, a different method was used.

The data was analysed via taking the data and splitting it up into 20 s chunks, which were than Fourier transformed to extract out the amplitude of the resonance frequency,

utilising the fact that the magnitude of the Fourier transform is directly proportional to the strength of the sine plus cosine waves of the frequency in question. The resonance frequency was extracted via the peaks in the Fourier transform. This method was compared to the traditional lock in method, and was found to have computational advantages in speed, without sacrificing accuracy.

6.7.1 Lock in Amplifier

The lock in amplifier works by extracting the amplitude of a frequency via the orthogonality of the sines and cosines. By multiplying a sine wave at the same frequency of the resonance frequency (or any frequency you want to extract) over a reasonably long period of time, the other frequencies drop out. Consider the following equations:

$$\begin{aligned} X =& \frac{1}{t_a}\int_t^{t+t_a} \sin\left(2\pi f_0 t'\right) x\left(t'\right) dt' \\ \simeq& \frac{1}{t_a}\int_t^{t+t_a} \sin\left(2\pi f_0 t'\right) x_0\left(t'\right) \sin\left(2\pi f_0 t' + \beta\right) dt' \\ =& \frac{1}{t_a}\int_t^{t+t_a} \sin\left(2\pi f_0 t'\right) x_0\left(t'\right) \left(\sin\left(2\pi f_0 t'\right)\cos\beta + \cos\left(2\pi f_0 t'\right)\sin\beta\right) dt' \\ \simeq& \frac{1}{t_a}\int_t^{t+t_a} \sin\left(2\pi f_0 t'\right) x_0\left(t'\right) \sin\left(2\pi f_0 t'\right)\cos\beta dt' \\ \simeq& \frac{1}{2} x_0\left(t\right)\cos\left(\beta\right) \end{aligned} \tag{6.4}$$

and similarly

$$Y = \frac{1}{t_a}\int_t^{t+t_a} \cos\left(2\pi f_0 t'\right) x\left(t'\right) dt' \simeq \frac{1}{2} x_0\left(t\right)\sin\left(\beta\right), \tag{6.5}$$

where $t_a \gg \frac{1}{f_0}$ is the averaging time, $x\left(t\right)$ the original signal, $x_0\left(t\right)$ the amplitude of the original signal at the frequency f_0 and β the phase angle between the signal and the sine wave. Combining the two equations, we get

$$x_0\left(t\right) = 2\sqrt{X^2 + Y^2}, \tag{6.6}$$

which is the amplitude at f_0 of the initial signal.

The astute reader may ask for the need to calculate both X and Y; after all, either X or Y are directly proportional to $x_0\left(t\right)$. Unfortunately, the phase angle β will change from each set of t_a chosen, unless t_a is taken as an integer multiple of $\frac{1}{f_0}$. However, even if t_a is chosen thusly, the discreteness of the data sampling will guarantee a drift of β, unless

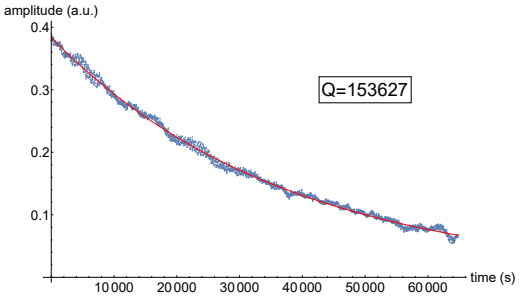

(A) Plot t_a of 20 s using the lock in method, with interpolation order 0 (rectangular method), with fitted exponential curve, with the calculated Q shown

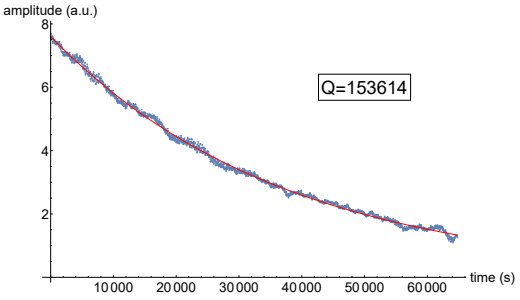

(B) plot t_a of 20 s using Fourier transform chunking, with fitted exponential curve, with the calculated Q shown. Note how there is less noise here.

FIGURE 6.6: Plots for the same C-axis sapphire fibre ringdown, comparing the lock in method with Fourier transform chunking. The ringdown used is the same as in fig 6.2. We see that the two methods are very comparable, but with the ringdown method being slightly more noisy. As conceptually they are identical, this additional noise can be attributed to the use of the rectangular method to perform numerical integration, which was used due to computational ease. t_a of 20 s was chosen for both Q. The sample rate for this data is 100 samples per second.

steps are taken to correct for it. By calculating both X and Y, we are free to choose t_a freely, as long as it is significantly longer than $\frac{1}{f_0}$.

In practice, this method is computationally intensive, due to the requirement of integrating a data series, which requires an interpolation function. Considering that our data sampling of 100 to 400 samples per second, taken over a day, extracting the amplitude this way is not practical. If interpolation is not done, and a simple summation is used, it results in a computationally quick calculation, but with some errors.

6.7.2 Fourier Transform Chunking

The method used for analysis shall be called Fourier transform chunking. This method uses the same orthogonality of the sines and cosines, but leverages on the computational speed of the fast Fourier transform (FFT) to do the calculation. The data is split into chunks t_a, which has the FFT applied to it. The value corresponding to the frequency of interest in then picked out, which is proportional to the amplitude of the signal strength, with the exact proportionality constant depending on the Fourier transform definition used. To wit,

$$n = round(f_0 t_a + 1), \tag{6.7}$$

where n is the nth number of the FFT and corresponds to the frequency f_0, and $round()$ refers to rounding to the closest integer.

As a refresher, the Fourier transform is given by

$$\hat{x}(f) = \int_{-\infty}^{\infty} x(t) e^{-2\pi i t f} dt = \int_{-\infty}^{\infty} x(t) \left(\cos(2\pi t f) - i \sin(2\pi t f)\right) dt, \tag{6.8}$$

which, due to the orthogonality of the sines and cosines, gives you a real part corresponding to the amplitude of the cosine part of the frequency in question and an imaginary part for the amplitude of the sine part, which means that taking the amplitude gives you something proportional to the strength of the frequency in question.

Granted, errors can creep in via the edge effects of the truncated signal, and that the signal frequency resolution is limited to

$$\Delta f = \frac{1}{t_a}. \tag{6.9}$$

This becomes of great importance when there are peaks close to each other. In those cases, t_a must be chosen large enough so as to remove overlap. Figure 6.6 shows the comparison between different t_a values for both the lock in method and the Fourier transform chunking method, using a data set collected. Figure 6.7 shows a ringdown with a large range of t_a applied. We see that the results are very stable and that the choice of 20 s is as good as any.

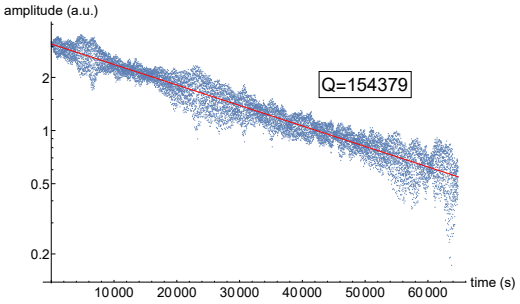

(A) Logplot t_a of 5 s, with fitted exponential curve, with the calculated Q shown

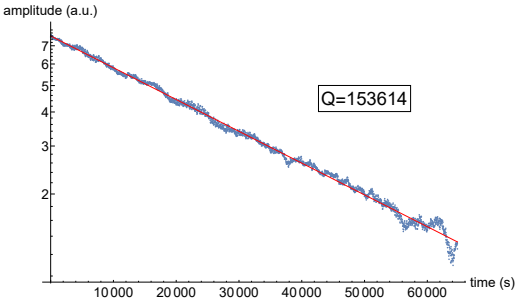

(B) Logplot t_a of 20 s, with fitted exponential curve, with the calculated Q shown

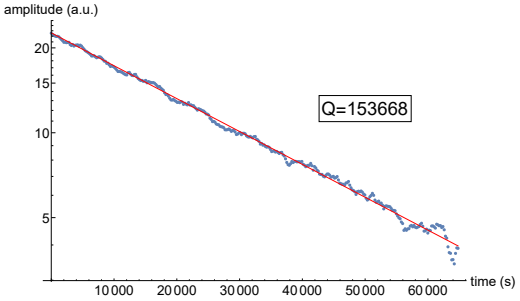

(C) Logplot t_a of 200 s, with fitted exponential curve, with the calculated Q shown

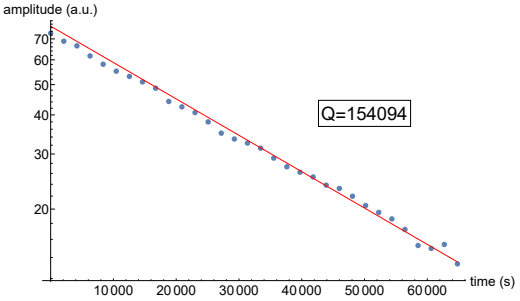

(D) Logplot t_a of 2000 s, with fitted exponential curve, with the calculated Q shown

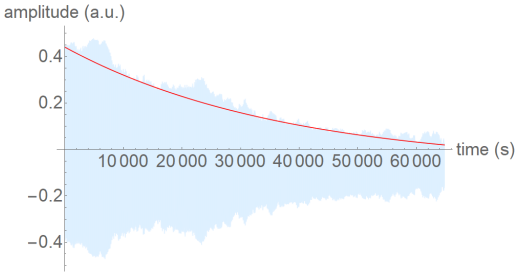

(E) Raw data with the exponential fit from t_a of 20 s overlaid. The individual oscillations are impossible to see at this scale, as one cycle is less than a second.

FIGURE 6.7: Logplots for the same C-axis sapphire fibre ringdown as 6.6 and 6.6, with different averaging times t_a, ranging from 5 s to 2000 s. The frequency of this ringdown is 1.31 Hz. We see that the results are very robust with the calculated Q barely changing. t_a of 20 s was chosen for the calculation of Q, and is superpositioned apon the raw data in (E). The sample rate for this data is 100 samples per second.

Chapter 7

Conclusion

7.1 Summary

We have experimentally verified that sapphire fibres in torsion, are not limited by thermoelastic damping like their flexural counterparts. This has allowed for an order of magnitude increase in measured Q, which shows that sapphire is a viable material for room temperature torsion pendulums. Nonetheless, fused silica might probably be still the better choice, due to it being a better studied material. However, this is not an option for cryogenic temperatures, due to the peak in loss at lower temperatures. We have also demonstrated here an order of magnitude improvement of Q over metal fibres of similar dimensions [30], which might prove critical for precision experiments. While the requirement of TOBA is still three orders of magnitudes away, we have measured the highest fibre Q of sapphire at room temperature. This is also the highest Q for sapphire measured at low frequencies of around 1 Hz at room temperatures. This measurement is agrees with the data in [7], and shows that we have likely achieved the limit for an unpolished sapphire fibre. It also lends credence to the idea that the surface loss is frequency independent over a large range of frequencies. Unfortunately, for our current measurements of a polished fibre, we were likely limited by clamp losses, and thus unable to achieve a better result. Improving on this would be the next step going forward.

7.2 Future Work

The current work done is just a small fraction of what is planned. In order to unlock the full potential of crystal fibres and increase its viability in use on experiments, further work has to be done.

7.2.1 Clamp Loss

Clamp loss is a perennial bugbear in terms of thermal noise and Q measurements. It is also likely to be the cause of the polished fibre not reaching a higher Q than the unpolished samples. Generally, monolithic system replacing simple clamps is required to achieve a Q close to that of the crystalline wire bulk. Thus, for TOBA, a monolithic or semi-monolithic system would probably be required to achieve the goal of $Q \sim 10^8$. There has already been some studies on bonding for sapphire [70, 71], and KAGRA utilises HCB to achieve its monolithic suspension. However, for experiments that require a better Q than what metals can provide but not require such a strict requirement, sapphire is a viable choice, even with the simple clamps used in this experiment. Note that the actual clamp loss mechanism in torsion pendulums probably differ from standard pendulums in some way, and merits a deeper study. The first would be to quantify the clamp loss by measuring how Q changes with clamp strength. This study would also let us quantify the breaking strength of current samples, apart from the C-axis samples, which has already been tested to break at a torque strength of 1.2 Nm for the current clamp design.

7.2.2 Surface Loss Studies

As surface losses are the penultimate limiting factor of Q for crystal fibres, an investigation to quantify and minimise it is essential. To do so, in addition to the current 1 mm thick wires, 10 mm long sapphire wires polished to a scratch-dig specification 80-50, which is a US military specification defining optical quality [72], was sourced from Orbe Pioneer with thickness ranging from 1 mm to 3 mm. These will be used to measure the relation between Q and the surface quality via the surface to volume ratio. As all these samples are sourced from the same company, presumably the differences in the bulk and the surface quality will be minimal. These samples will be measured once clamp loss has been found to be reduced till it no longer is a limiting factor.

Following that, surface treatments like chemical etching, further polishing, or even different growth methods will be studied to see if fibre Q can be increased further. Considering that surface quality is also the key to the tensile strength of crystals, improving on the quality would allow for thinner suspensions, thus reducing suspension thermal noise even further.

7.2.3 Cryogenic Cooling

As mentioned in chapter 2, TOBA is designed to run at cryogenic temperatures, to lower thermal noise. In addition to lower temperatures leading directly to lower thermal noise, Q itself is often improved by orders of magnitude, across a variety of materials [5, 6, 34, 47]. Generally, fibres show even larger improvement, due to a reduction in additional losses like the thermoelastic effect.

On the other hand, there are materials that show drops in Q at specific temperature ranges, with the most famous being fused silica [38], which is the reason for its non-suitability as a low loss candidate material for low loss systems. Sapphire has not shown any such peaks in loss [10, 47], except small increases at around 150 K and 30 K. Characterising the Q of sapphire fibres as a function of temperature would be a worthwhile study, once clamp losses can be brought under control, and a comparison can be then made against [10].

This experiments were designed with cryogenic cooling in mind, with the clamps made of copper beryllium, which is known to have low internal friction and high strength for copper alloy and maintains a high Q at cryogenic temperatures.

7.2.4 Different Materials

There are other crystalline materials that offer low loss, with a well studied alternative being silicon. Cantilever modes of silicon have been studied, and there have been measured increases of Q from 10^4 to 10^7[51] when the sample was cooled to cryogenic temperatures. Bulk silicon has also shown performance similar to sapphire, and should perform similarly. There might be advantages in terms on tapping the semi-conductor industry's expertise in growing pure silicon, as purity would be a key element in determining bulk Q.

7.2.5 Crystal Properties

Further study of crystal properties should also be conducted. Proper understanding of how the anisotropy of the crystals affect the mechanical loss of the system deserves a deeper look, as there are complexities hinted at in [10] on this topic. Understanding the different loss mechanisms will allow us the understand the limits of crystals, and that would allow us to study how deviations from the perfect crystal lattice, for example, would lead to changes in Q. This would allow for analysing how much high temperature annealing ($\sim$ 2000°C) would help in improving Q, as this would mainly affect bulk Q.

Appendix A

Dilution factor

The dilution factor, which is how much the Q of a pendulum relates to the Q of the suspension fibre, is often given as $\frac{2mgL}{\sqrt{F_t Y J}}$ [29, 65]. Unfortunately, one of the assumptions embedded in the derivation of the equation is that the length of the pendulum and the effective length of the pendulum are similar. See fig A.1 for more details. Here, we remove that assumption, creating a more general form of the dilution factor, one that is applicable to this work.

Following the work in [65], we first start out with the deformation of the fibre as

$$y(x) = \frac{Fd}{F_T}\left(e^{-\frac{x}{d}} + \frac{x}{d} - 1\right), \tag{A.1}$$

where $d = \sqrt{\frac{YJ}{F_T}}$, x the vertical position, y the horizontal position, F_T the downwards tension and F the displacement force horizontally. The origin for the coordinate used is the clamp point of the fibre with the celling.

The relation between the projection of the fibre on the vertical axis L_x is given by

$$L = \int_0^{L_x} \sqrt{1 + \left(\frac{dy}{dx}\right)^2}\, dx \simeq \int_0^{L_x} 1 + \frac{1}{2}\left(\frac{dy}{dx}\right)^2 dx, \tag{A.2}$$

which is simply the arc length equation, along with the assumption of small displacements, $\frac{dy}{dx} < 1$, allowing for a simplification via binomial expansion. To evaluate it, we first need

$$\frac{dy}{dx} = \frac{F}{F_T}\left(1 - e^{-\frac{x}{d}}\right), \tag{A.3}$$

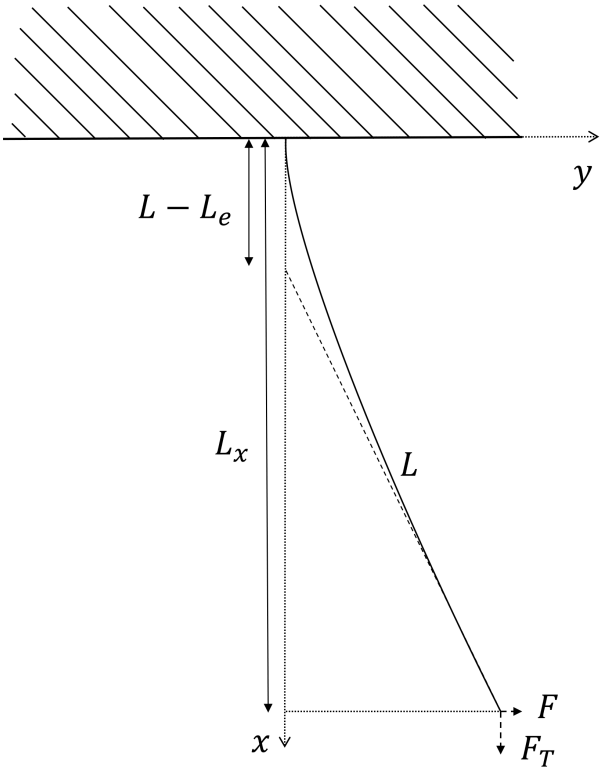

FIGURE A.1: Illustration of a bending fibre subjected to tension F_T and a displacement force F, without the assumption that the effective length L_e of the pendulum is approximately the same as the real length L. L_x is the fibre projected on the vertical (x) axis.

which we use and get

$$\begin{aligned} L &\simeq \int_0^{L_x} 1 + \frac{1}{2}\left(\frac{F}{F_T}\left(1 - e^{-\frac{x}{d}}\right)\right)^2 dx \\ &= \int_0^{L_x} 1 + \frac{1}{2}\left(\frac{F}{F_T}\right)^2 \left(1 - 2e^{-\frac{x}{d}} + e^{-\frac{2x}{d}}\right) dx \\ &= L_x + \left(\frac{F}{F_T}\right)^2 \left(\frac{L_x}{2} + de^{-\frac{L_x}{d}} - d - \frac{d}{4}e^{-\frac{2L_x}{d}} + \frac{d}{4}\right) \\ &= L_x + \left(\frac{F}{F_T}\right)^2 \left(\frac{L_x}{2} - \frac{3d}{4} + de^{-\frac{L_x}{d}} - \frac{d}{4}e^{-\frac{2L_x}{d}}\right). \end{aligned} \tag{A.4}$$

Now, the elastic potential energy of a slightly bent rod is given by [65, 73]

$$E_e = \frac{1}{2}EJ \int_0^{L_x} \left(\frac{d^2y}{dx^2}\right)^2 dx, \tag{A.5}$$

and in our case,

$$\frac{d^2y}{dx^2} = \frac{F}{F_T d}\left(e^{-\frac{x}{d}}\right), \tag{A.6}$$

thus giving

$$E_e = \frac{1}{2}EJ\int_0^{L_x}\left(\frac{F}{F_T d}\left(e^{-\frac{x}{d}}\right)\right)^2 dx. \tag{A.7}$$

The gravitational potential energy is simply given by

$$E_g = mg(L - L_x) = \frac{T}{n}(L - L_x), \tag{A.8}$$

where n is the number of wires the mass is being held by.

The dilution factor is given by $\frac{E_g+E_e}{E_e}$, because

$$\begin{aligned} Q_{pendulum} &= 2\pi\frac{E}{\Delta E} = 2\pi\frac{E_g + E_e}{\Delta E_g + \Delta E_e} \\ &= 2\pi\frac{E_e}{\Delta E_e}\frac{E_g + E_e}{E_e} = Q_{fibre}\frac{E_g + E_e}{E_e}, \end{aligned} \tag{A.9}$$

where we assume gravity does not dissipate energy to any significant extent.

The above equations can then be simply numerically solved, giving a dilution factor of 4.1 for our standard setup, and 2.1 for the low mass setup. In comparison, the standard formula, gives a value of 6.0 and 3.3 respectively. Note that F is undetermined, but it should cancel out, so any reasonably small number (but not too small as to induce floating point errors) can be chosen. We have determined that the dilution factor is stable for values of F over many orders of magnitude.

For completeness, we would like to derive the effective length of the pendulum, which is shown in figure 6.4 to be shorten by $\sim d$.

Now, we have

$$y(L_x) = \frac{Fd}{F_T}\left(e^{-\frac{L_x}{d}} + \frac{L_x}{d} - 1\right), \tag{A.10}$$

which is the deflection in the horizontal direction at the end of the fibre, and

$$\frac{dy}{dx}(L_x) = \frac{F}{F_T}\left(1 - e^{-\frac{L_x}{d}}\right), \tag{A.11}$$

which is the gradient at the end of the fibre.

The projection of the effective length of the fibre on the vertical is then given by

$$(L_e)_x = \frac{y(L_x)}{\frac{dy}{dx}(L_x)} = \frac{L_x}{1 - e^{-\frac{L_x}{d}}} - d, \tag{A.12}$$

which means that for small deflections,

$$L_e \simeq \frac{L}{1 - e^{-\frac{L}{d}}} - d, \tag{A.13}$$

with the shortening being

$$L - L_e \simeq L - \frac{L}{1 - e^{-\frac{L}{d}}} + d, \tag{A.14}$$

which still holds even if $d > L$. In the case of $\frac{L}{d} \gg 1$, it becomes

$$L - L_e \simeq d. \tag{A.15}$$

Thus, the need for this more complex form of the dilution factor is only required when the assumption $\frac{L}{d} \gg 1$ does not hold.

References

[1] H. Cavendish, "Experiments to Determine the Density of the Earth," *Philosophical Transactions of the Royal Society of London*, vol. 88, pp. 469–526, 1798.

[2] M. Hueller, A. Cavalleri, R. Dolesi, S. Vitale, and W. J. Weber, "Torsion pendulum facility for ground testing of gravitational sensors for LISA," *Classical and Quantum Gravity*, vol. 19, no. 7, p. 1757, 2002.

[3] R. Newman, M. Bantel, E. Berg, and W. Cross, "A measurement of G with a cryogenic torsion pendulum," *Philosophical Transactions of the Royal Society of London A: Mathematical, Physical and Engineering Sciences*, vol. 372, no. 2026, 2014.

[4] M. Ando, K. Ishidoshiro, K. Yamamoto, K. Yagi, W. Kokuyama, K. Tsubono, and A. Takamori, "Torsion-bar antenna for low-frequency gravitational-wave observations," *Phys. Rev. Lett.*, vol. 105, p. 161101, Oct 2010.

[5] W. Duffy, "Acoustic quality factor of copper, brass and beryllium copper from 50 mK to 300 K," *Cryogenics*, vol. 32, no. 12, pp. 1121 – 1124, 1992.

[6] W. Duffy, "Acoustic quality factor of molybdenum and tungsten at low temperatures," *Journal of Applied Physics*, vol. 72, no. 12, pp. 5628–5634, 1992.

[7] K. Numata, G. B. Bianc, M. Tanaka, S. Otsuka, K. Kawabe, M. Ando, and K. Tsubono, "Measurement of the mechanical loss of crystalline samples using a nodal support," *Physics Letters A*, vol. 284, no. 4, pp. 162 – 171, 2001.

[8] S. Rowan, G. Cagnoli, P. Sneddon, J. Hough, R. Route, E. Gustafson, M. Fejer, and V. Mitrofanov, "Investigation of mechanical loss factors of some candidate materials for the test masses of gravitational wave detectors," *Physics Letters A*, vol. 265, no. 1, pp. 5 – 11, 2000.

[9] A. V. Cumming, A. S. Bell, L. Barsotti, M. A. Barton, G. Cagnoli, D. Cook, L. Cunningham, M. Evans, G. D. Hammond, G. M. Harry, A. Heptonstall, J. Hough, R. Jones, R. Kumar, R. Mittleman, N. A. Robertson, S. Rowan, B. Shapiro, K. A. Strain, K. Tokmakov, C. Torrie, and A. A. van Veggel, "Design and development of the advanced LIGO monolithic fused silica suspension," *Classical and Quantum Gravity*, vol. 29, no. 3, p. 035003, 2012.

[10] V. B. Braginsky, V. P. Mitrofanov, and V. I. Panov, *Systems with Small Dissipation*. 1985.

[11] K. Numata, G. B. Bianc, N. Ohishi, A. Sekiya, S. Otsuka, K. Kawabe, M. Ando, and K. Tsubono, "Measurement of the intrinsic mechanical loss of low-loss samples using a nodal support," *Physics Letters A*, vol. 276, no. 1, pp. 37 – 46, 2000.

[12] B. P. Abbott *et al.*, "Observation of gravitational waves from a binary black hole merger," *Phys. Rev. Lett.*, vol. 116, p. 061102, Feb 2016.

[13] J. Aasi *et al.*, "Advanced LIGO," *Classical and Quantum Gravity*, vol. 32, no. 7, p. 074001, 2015.

[14] Y. Kuwahara, A. Shoda, K. Eda, and M. Ando, "Search for a stochastic gravitational wave background at 1–5 hz with a torsion-bar antenna," *Phys. Rev. D*, vol. 94, p. 042003, Aug 2016.

[15] K. Danzmann *et al.*, "Laser Interferometer Space Antenna," *ESA L3 proposal*, Feb. 2017.

[16] S. Sato *et al.*, "DECIGO: The japanese space gravitational wave antenna," *Journal of Physics: Conference Series*, vol. 154, no. 1, p. 012040, 2009.

[17] T. Shimoda, N. Aritomi, A. Shoda, Y. Michimura, and M. Ando, "Seismic cross-coupling noise in torsion pendulums," *Phys. Rev. D*, vol. 97, p. 104003, May 2018.

[18] P. J. Mohr, D. B. Newell, and B. N. Taylor, "CODATA Recommended Values of the Fundamental Physical Constants: 2014," *Rev. Mod. Phys.*, vol. 88, no. 3, p. 035009, 2016.

[19] P. R. Heyl, "A redetermination of the constant of gravitation," *Bureau of Standards Journal of Research*, vol. 5, pp. 1243 – 1290, Dec 1930.

[20] P. R. Heyl and P. Chrzanowski, "A new determination of the constant of gravitation," *Bureau of Standards Journal of Research*, vol. 29, Jul 1942.

[21] Q. Li, J.-P. Liu, H.-H. Zhao, S.-Q. Yang, L.-C. Tu, Q. Liu, C.-G. Shao, Z.-K. Hu, V. Milyukov, and J. Luo, "G measurements with time-of-swing method at HUST," *Philosophical Transactions of the Royal Society of London A: Mathematical, Physical and Engineering Sciences*, vol. 372, no. 2026, 2014.

[22] K. Kuroda, "Does the time-of-swing method give a correct value of the newtonian gravitational constant?," *Phys. Rev. Lett.*, vol. 75, pp. 2796–2798, Oct 1995.

[23] M. Bantel and R. Newman, "High precision measurement of torsion fiber internal friction at cryogenic temperatures," *Journal of Alloys and Compounds*, vol. 310, no. 1, pp. 233 – 242, 2000. Intern. Conf. Internal Friction and Ultrasonic Attentuation in Solids (ICIFUAS-12).

[24] H. Nyquist, "Thermal agitation of electric charge in conductors," *Physics Review*, vol. 32, pp. 110–113, Jul 1928.

[25] H. B. Callen and T. A. Welton, "Irreversibility and generalized noise," *Physics Review*, vol. 83, pp. 34–40, Jul 1951.

[26] E. I. Green, "The story of Q," *American Scientist*, vol. 43, no. 4, pp. 584–594, 1955.

[27] A. L. Kimball and D. E. Lovell, "Internal friction in solids," *Phys. Rev.*, vol. 30, pp. 948–959, Dec 1927.

[28] Z.-K. Hu and J. Luo, "Amplitude dependence of quality factor of the torsion pendulum," *Physics Letters A*, vol. 268, no. 4, pp. 255 – 259, 2000.

[29] P. R. Saulson, "Thermal noise in mechanical experiments," *Phys. Rev. D*, vol. 42, pp. 2437–2445, Oct 1990.

[30] G. Cagnoli, L. Gammaitoni, J. Kovalik, F. Marchesoni, and M. Punturo, "Low-frequency internal friction in clamped-free thin wires," *Physics Letters A*, vol. 255, no. 4, pp. 230 – 235, 1999.

[31] J. Weber, "Observation of the thermal fluctuations of a gravitational-wave detector," *Phys. Rev. Lett.*, vol. 17, pp. 1228–1230, Dec 1966.

[32] J. Weber, "Gravitational radiation," *Phys. Rev. Lett.*, vol. 18, pp. 498–501, Mar 1967.

[33] J. Weber, "Gravitational-wave-detector events," *Phys. Rev. Lett.*, vol. 20, pp. 1307–1308, Jun 1968.

[34] T. Suzuki, K. Tsubono, and H. Hirakawa, "Quality factor of vibration of aluminum alloy disks," *Physics Letters A*, vol. 67, no. 1, pp. 2 – 4, 1978.

[35] W. Duffy, "Acoustic quality factor of aluminum alloys from 50 mK to 300 K," *Journal of Applied Physics*, vol. 68, no. 11, pp. 5601–5609, 1990.

[36] W. Duffy and R. Umstattd, "Acoustic quality factor of niobium and vanadium at low temperatures," *Journal of Applied Physics*, vol. 75, no. 9, pp. 4489–4495, 1994.

[37] A. Ageev, B. C. Palmer, A. D. Felice, S. D. Penn, and P. R. Saulson, "Very high quality factor measured in annealed fused silica," *Classical and Quantum Gravity*, vol. 21, no. 16, p. 3887, 2004.

[38] A. Schroeter, R. Nawrodt, R. Schnabel, S. Reid, I. Martin, S. Rowan, C. Schwarz, T. Koettig, R. Neubert, M. Thürk, W. Vodel, A. Tünnermann, K. Danzmann, and P. Seidel, "On the mechanical quality factors of cryogenic test masses from fused silica and crystalline quartz," *ArXiv e-prints*, Sept. 2007.

[39] D. F. McGuigan, C. C. Lam, R. Q. Gram, A. W. Hoffman, D. H. Douglass, and H. W. Gutche, "Measurements of the mechanical Q of single-crystal silicon at low temperatures," *Journal of Low Temperature Physics*, vol. 30, no. 5-6, pp. 621–629, 1978.

[40] J. Luo, Q. Liu, L.-C. Tu, C.-G. Shao, L.-X. Liu, S.-Q. Yang, Q. Li, and Y.-T. Zhang, "Determination of the newtonian gravitational constant g with time-of-swing method," *Phys. Rev. Lett.*, vol. 102, p. 240801, Jun 2009.

[41] K. Numata, J. Horowitz, and J. Camp, "Coated fused silica fibers for enhanced sensitivity torsion pendulum for LISA," *Physics Letters A*, vol. 370, no. 2, pp. 91 – 98, 2007.

[42] V. B. Braginskii, V. P. Mitrofanov, and O. A. Okhrimenko, "Oscillators for free-mass gravitational-wave antennas," *Pisma v Zhurnal Eksperimentalnoi i Teoreticheskoi Fiziki*, vol. 55, pp. 424–426, Apr. 1992.

[43] H. Liebowitz, *Fracture : an advanced treatise*. New York : Academic Press, 1968. V. 7.

[44] P. Amico, L. Bosi, L. Carbone, L. Gammaitoni, F. Marchesoni, M. Punturo, F. Travasso, and H. Vocca, "Monolithic fused silica suspension for the virgo gravitational waves detector," *Review of Scientific Instruments*, vol. 73, no. 9, pp. 3318–3323, 2002.

[45] B. Willke *et al.*, "The GEO 600 gravitational wave detector," *Classical and Quantum Gravity*, vol. 19, no. 7, p. 1377, 2002.

[46] A. Cavalleri, G. Ciani, R. Dolesi, A. Heptonstall, M. Hueller, D. Nicolodi, S. Rowan, D. Tombolato, S. Vitale, P. J. Wass, and W. J. Weber, "A new torsion pendulum for testing the limits of free-fall for LISA test masses," *Classical and Quantum Gravity*, vol. 26, no. 9, p. 094017, 2009.

[47] T. Uchiyama, T. Tomaru, M. Tobar, D. Tatsumi, S. Miyoki, M. Ohashi, K. Kuroda, T. Suzuki, N. Sato, T. Haruyama, A. Yamamoto, and T. Shintomi, "Mechanical quality factor of a cryogenic sapphire test mass for gravitational wave detectors," *Physics Letters A*, vol. 261, no. 1, pp. 5 – 11, 1999.

[48] T. Uchiyama, T. Tomaru, D. Tatsumi, S. Miyoki, M. Ohashi, K. Kuroda, T. Suzuki, A. Yamamoto, and T. Shintomi, "Mechanical quality factor of a sapphire fiber at cryogenic temperatures," *Physics Letters A*, vol. 273, no. 5, pp. 310 – 315, 2000.

[49] J. Kovalik and P. R. Saulson, "Mechanical loss in fibers for low noise pendulums," *Review of Scientific Instruments*, vol. 64, no. 10, pp. 2942–2946, 1993.

[50] S. D. Penn, G. M. Harry, A. M. Gretarsson, S. E. Kittelberger, P. R. Saulson, J. J. Schiller, J. R. Smith, and S. O. Swords, "High quality factor measured in fused silica," *Review of Scientific Instruments*, vol. 72, no. 9, pp. 3670–3673, 2001.

[51] R. Nawrodt, C. Schwarz, S. Kroker, I. W. Martin, R. Bassiri, F. Brückner, L. Cunningham, G. D. Hammond, D. Heinert, J. Hough, T. Käsebier, E.-B. Kley, R. Neubert, S. Reid, S. Rowan, P. Seidel, and A. Tünnermann, "Investigation of mechanical losses of thin silicon flexures at low temperatures," *Classical and Quantum Gravity*, vol. 30, no. 11, p. 115008, 2013.

[52] A. M. Gretarsson and G. M. Harry, "Dissipation of mechanical energy in fused silica fibers," *Review of Scientific Instruments*, vol. 70, no. 10, pp. 4081–4087, 1999.

[53] I. A. Bilenko, V. B. Braginsky, and S. L. Lourie, "Mechanical losses in thin fused silica fibres," *Classical and Quantum Gravity*, vol. 21, no. 5, p. S1231, 2004.

[54] D. W. Carr, S. Evoy, L. Sekaric, H. G. Craighead, and J. M. Parpia, "Measurement of mechanical resonance and losses in nanometer scale silicon wires," *Applied Physics Letters*, vol. 75, no. 7, pp. 920–922, 1999.

[55] C. Zener, "Internal friction in solids. i. theory of internal friction in reeds," *Phys. Rev.*, vol. 52, pp. 230–235, Aug 1937.

[56] C. Zener, "Internal friction in solids ii. general theory of thermoelastic internal friction," *Phys. Rev.*, vol. 53, pp. 90–99, Jan 1938.

[57] V. B. Braginsky and A. B. Manukin, *Measurement of weak forces in physics experiments*. 1977.

[58] V. Braginsky, V. Mitrofanov, and O. Okhrimenko, "The isolation of test masses for gravitational wave antennae," *Physics Letters A*, vol. 175, no. 2, pp. 82 – 84, 1993.

[59] S. Rowan, S. Twyford, R. Hutchins, J. Kovalik, J. Logan, A. McLaren, N. Robertson, and J. Hough, "Q factor measurements on prototype fused quartz pendulum suspensions for use in gravitational wave detectors," *Physics Letters A*, vol. 233, no. 4, pp. 303 – 308, 1997.

[60] G. Cagnoli, L. Gammaitoni, J. Hough, J. Kovalik, S. McIntosh, M. Punturo, and S. Rowan, "Very high Q measurements on a fused silica monolithic pendulum for use in enhanced gravity wave detectors," *Phys. Rev. Lett.*, vol. 85, pp. 2442–2445, Sep 2000.

[61] M. Lorenzini, *Suspension Thermal Noise Issues for Advanced GW Interferometric Detectors*. PhD thesis, University of Florence, 2007.

[62] G. Cagnoli, L. Gammaitoni, J. Kovalik, F. Marchesoni, and M. Punturo, "Suspension losses in low-frequency mechanical pendulums," *Physics Letters A*, vol. 213, no. 5, pp. 245 – 252, 1996.

[63] A. Gillespie and F. Raab, "Suspension losses in the pendula of laser interferometer gravitational-wave detectors," *Physics Letters A*, vol. 190, no. 3, pp. 213 – 220, 1994.

[64] B. P. Abbott *et al.*, "LIGO: The Laser interferometer gravitational-wave observatory," *Rept. Prog. Phys.*, vol. 72, p. 076901, 2009.

[65] G. Cagnoli, J. Hough, D. DeBra, M. Fejer, E. Gustafson, S. Rowan, and V. Mitrofanov, "Damping dilution factor for a pendulum in an interferometric gravitational waves detector," *Physics Letters A*, vol. 272, no. 1, pp. 39 – 45, 2000.

[66] T. Quinn, C. Speake, R. Davis, and W. Tew, "Stress-dependent damping in cube torsion and flexure suspensions at stresses up to 1.1 gpa," *Physics Letters A*, vol. 197, no. 3, pp. 197 – 208, 1995.

[67] G. Cagnoli, L. Gammaitoni, J. Kovalik, F. Marchesoni, and M. Punturo, "Full scale prototype of high q pendulum for interferometric gravitational wave detectors," *Review of Scientific Instruments*, vol. 71, no. 5, pp. 2206–2210, 2000.

[68] Y. L. Huang and P. R. Saulson, "Dissipation mechanisms in pendulums and their implications for gravitational wave interferometers," *Review of Scientific Instruments*, vol. 69, no. 2, pp. 544–553, 1998.

[69] F. Travasso and V. Collaboration, "Status of the monolithic suspensions for advanced Virgo," *Journal of Physics: Conference Series*, vol. 957, no. 1, p. 012012, 2018.

[70] K. Haughian, R. Douglas, A. A. van Veggel, J. Hough, A. Khalaidovski, S. Rowan, T. Suzuki, and K. Yamamoto, "The effect of crystal orientation on the cryogenic strength of hydroxide catalysis bonded sapphire," *Classical and Quantum Gravity*, vol. 32, no. 7, p. 075013, 2015.

[71] A. Dari, F. Travasso, H. Vocca, and L. Gammaitoni, "Breaking strength tests on silicon and sapphire bondings for gravitational wave detectors," *Classical and Quantum Gravity*, vol. 27, no. 4, p. 045010, 2010.

[72] "MIL-PRF-13830B, optical components for fire control instruments; general specification governing the manufacture, assembly, and inspection of," *United States Military Standard, Performance Specification*, Sep 1963.

[73] L. D. Landau, L. P. Pitaevskii, A. M. Kosevich, and E. M. Lifshitz, *Theory of Elasticity*. Butterworth-Heinemann, 3 ed., Dec 2012.